Resource

Cell Host & Microbe

Global Reprogramming of Host Kinase Signaling in Response to Fungal Infection

Graphical Abstract

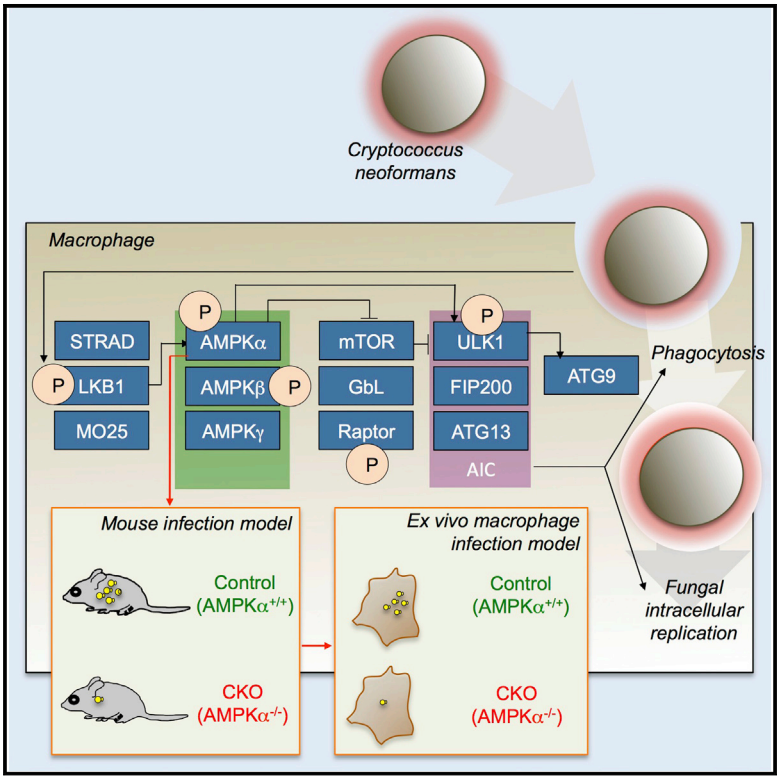

Highlights

- *C. neoformans* infection results in global reprogramming of host cell kinase cascades
- The host autophagy initiation complex confers susceptibility to fungal infection
- Recruitment of autophagy initiation components to phagosomes promotes fungal uptake
- Host AMPKα confers susceptibility to fungal infection in a murine cryptococcosis model

Authors

Aseem Pandey, Sheng Li Ding, Qing-Ming Qin, ..., William K. Russell, Thomas A. Ficht, Paul de Figueiredo

Correspondence

wirussel@utmb.edu (W.K.R.), tficht@tamu.edu (T.A.F.), pjdefigueiredo@tamu.edu (P.d.F.)

In Brief

Cryptococcus neoformans is a deadly fungal pathogen whose intracellular lifestyle is critical for virulence. Pandey et al. perform a global phosphoproteomic analysis of the host response to *C. neoformans* infection and reveal that the host autophagy initiation complex regulates intracellular parasitism.

Pandey et al., 2017, Cell Host & Microbe *21*, 637–649
May 10, 2017
http://dx.doi.org/10.1016/j.chom.2017.04.008

Cell Host & Microbe
Resource

Global Reprogramming of Host Kinase Signaling in Response to Fungal Infection

Aseem Pandey,[1,2,3,16] Sheng Li Ding,[1,2,15,16] Qing-Ming Qin,[4,5,16] Rahul Gupta,[6] Gabriel Gomez,[7] Furong Lin,[2] Xuehuan Feng,[1,2] Luciana Fachini da Costa,[1,2,3] Sankar P. Chaki,[3] Madhu Katepalli,[1] Elizabeth D. Case,[1] Erin J. van Schaik,[1] Tabasum Sidiq,[1] Omar Khalaf,[3] Angela Arenas,[3] Koichi S. Kobayashi,[1] James E. Samuel,[1] Gonzalo M. Rivera,[3] Robert C. Alaniz,[1] Sing-Hoi Sze,[8,9,10] Xiaoning Qian,[8,11] William J. Brown,[12] Allison Rice-Ficht,[13] William K. Russell,[14,*] Thomas A. Ficht,[3,*] and Paul de Figueiredo[1,2,3,17,*]

[1]Department of Microbial Pathogenesis and Immunology, Texas A&M Health Science Center, College Station, Texas 77843, USA
[2]Norman Borlaug Center, Texas A&M University, College Station, Texas 77843, USA
[3]Department of Veterinary Pathobiology, College of Veterinary Medicine, Texas A&M University, College Station, Texas 77843, USA
[4]College of Plant Sciences
[5]Key Laboratory of Zoonosis Research, Ministry of Education
Jilin University, Changchun 130062, Jilin, China
[6]Health and Engineering Group, Leidos Inc., 2295 Parklake Drive, Atlanta, GA 30345, USA
[7]Texas A&M Veterinary Medical Diagnostic Laboratory
[8]Center for Bioinformatics & Genomic Systems Engineering
[9]Department of Computer Science and Engineering, Dwight Look College of Engineering
[10]Department of Biochemistry & Biophysics
[11]Department of Electrical and Computer Engineering, Dwight Look College of Engineering
Texas A&M University, College Station, Texas 77843, USA
[12]Department of Molecular Biology and Genetics, Cornell University, Ithaca, NY 14853-2703, USA
[13]Department of Molecular and Cellular Medicine, College of Medicine, Texas A&M Health Science Center, College Station, Texas 77843, USA
[14]Department of Biochemistry and Molecular Biology, University of Texas Medical Branch, Galveston, TX 77555, USA
[15]Department of Plant Pathology, College of Plant Protection, Henan Agricultural University, Zhengzhou 450002, Henan, China
[16]These authors contributed equally
[17]Lead contact
*Correspondence: wirussel@utmb.edu (W.K.R.), tficht@tamu.edu (T.A.F.), pjdefigueiredo@tamu.edu (P.d.F.)
http://dx.doi.org/10.1016/j.chom.2017.04.008

SUMMARY

Cryptococcus neoformans (Cn) is a deadly fungal pathogen whose intracellular lifestyle is important for virulence. Host mechanisms controlling fungal phagocytosis and replication remain obscure. Here, we perform a global phosphoproteomic analysis of the host response to *Cryptococcus* infection. Our analysis reveals numerous and diverse host proteins that are differentially phosphorylated following fungal ingestion by macrophages, thereby indicating global reprogramming of host kinase signaling. Notably, phagocytosis of the pathogen activates the host autophagy initiation complex (AIC) and the upstream regulatory components LKB1 and AMPKα, which regulate autophagy induction through their kinase activities. Deletion of *Prkaa1*, the gene encoding AMPKα1, in monocytes results in resistance to fungal colonization of mice. Finally, the recruitment of AIC components to nascent *Cryptococcus*-containing vacuoles (CnCVs) regulates the intracellular trafficking and replication of the pathogen. These findings demonstrate that host AIC regulatory networks confer susceptibility to infection and establish a proteomic resource for elucidating host mechanisms that regulate fungal intracellular parasitism.

INTRODUCTION

Cn has emerged as the major causative agent of fungal meningoencephalitis worldwide, with more than million new cases of cryptococcosis reported annually and an alarming 60% fatality rate (Sabiiti and May, 2012). Cn is also a persistent threat to immunocompromised individuals, including HIV patients. The fungus resides in various environmental niches, and inhalation of fungal spores from the environment can lead to human infection (Sabiiti and May, 2012).

Autophagy is an evolutionarily conserved, "self-eating" program that cannibalizes organelles and intracellular nutrients to promote the survival of starved cells. The most common form of autophagy, macroautophagy (henceforth, "autophagy"), is characterized by the formation of a membrane-bounded compartment, the autophagosome, which engulfs substrates and transports them to the vacuole or lysosome for breakdown and recycling (Klionsky et al., 2016). In mammalian cells, the autophagy initiation complex (AIC)—an assembly that includes ULK1, ATG13, and FIP200 as well as ATG9, a transmembrane protein that organizes the preautophagosomal structure (phagophore)—plays pivotal roles during the early steps of autophagy induction (Jung et al., 2009). Various forms of

autophagic processes have been described, including xenophagy, which contributes to the control of intracellular vacuolar pathogens.

The signaling pathways that regulate autophagy initiation are not fully understood. However, the energy-sensing kinase AMPK plays an important role. AMPK is an evolutionarily conserved trimeric enzyme (with α, β, and Y subunits) that regulates cellular energy homeostasis and early steps in autophagosome biogenesis. The AMPK complex is activated either by increases in cellular AMP or ADP or by phosphorylation on Thr172 by CamKK-β, LKB1, or TAK1 (Hawley et al., 2005; Woods et al., 2003; Xie et al., 2006a), which stimulates a 100-fold increase in the kinase activity of the complex. This enhanced activity, in turn, controls signaling pathways that regulate important cellular phenomena, including protein synthesis, cell division and intracellular membrane trafficking. In eukaryotic cells, AMPK regulates autophagy (Mao and Klionsky, 2011).

Over the past several years, the mechanisms by which AMPK regulates autophagy have been illuminated. The AMPK complex (along with the mTORC1 complex) coordinately regulates autophagy by delivering opposing signals to the AIC. AMPK positively regulates autophagy induction through inhibition of mTORC1 while concomitantly regulating the phosphorylation of ULK1 and the activities of the downstream molecules ATG13, FIP200, and ATG101 (Alers et al., 2012), which coordinate the quality and strength of autophagy activation. AMPKα phosphorylation of ULK1 also controls ATG9 localization (Mack et al., 2012). In fact, the localization of ATG9 to autophagosomes requires ULK1- and AMPK-dependent phosphorylation of this protein (Weerasekara et al., 2014). Despite these advances, precise roles of host AIC components in regulating infection remain to be elucidated. Moreover, mechanisms that control interactions between host signaling pathways and intracellular fungal pathogens remain largely unknown.

Cn can survive, replicate, and persist in both intracellular and extracellular environments within mammalian hosts. Both lifestyles are important to pathogenesis; however, the molecular mechanisms that control intracellular parasitism remain obscure. Toward addressing this issue, we previously reported a functional analysis of host factors that regulate the internalization, intracellular replication, and nonlytic release of Cn from host cells (Qin et al., 2011). This work identified several proteins that regulate autophagy. We therefore hypothesized that a global phosphoproteomic analysis of the response of host cells to Cn infection would reveal additional roles for host autophagy proteins in regulating this process.

RESULTS

Phosphoproteomic Analysis of the Host Response to Fungal Infection

Initial events during infection of host cells by pathogens can guide the overall trajectory of infection and determine its ultimate outcome. However, these events remain poorly understood during interactions between fungal pathogens and mammalian host cells. To determine the initial biological response of murine macrophage cells (RAW264.7) to infection with Cn (strain H99), we used semiquantitative, label-free nano LC-MS/MS proteomic methods that have proven useful for elucidating the phosphoproteomic responses of host cells to bacterial pathogens (Schmutz et al., 2013). First, we infected host cells at a multiplicity of infection (MOI) of 10 with antibody-opsonized Cn for 2 hr, after which time greater than 60% of the host cells harbored the internalized fungus (Figure 1A). Lysates from 60 biologically independent samples of mock or infected host cells were then prepared using methods that isolated host proteins and limited capture and analysis of pathogen-derived components (Kim et al., 2012; Figure 1B). The lysates from each treatment were pooled and analyzed by LC-MS/MS in duplicate technical replicates to define the global proteome (Table S1) or phosphoproteome (Table S2) in response to fungal infection. After filtering low quality data, 5,614 and 5,268 phosphorylation sites (representing 2,531 and 2,505 gene products) were identified and quantified in the mock and infected samples, respectively (Figure 1C). A total of 2,076 phosphorylation sites (derived from 1,268 gene products) were deemed Cn-responsive, with 744 or 524 proteins increasing or decreasing by 1.5-fold or more, respectively, in total levels of phosphorylation upon infection. In the case of a protein possessing multiple phosphorylation sites, the total phosphorylation of the protein was used for analysis. The distribution of ratios for each proteomic or phosphoproteomic sample varied continuously, indicating no unexpected anomalies in the data (Figures 1D and 1E). The distribution of phosphorylated peptides displayed a strong bias (80.8%) toward single phosphorylations on serine or threonine residues (Table S2).

We analyzed proteins that were reprogrammed in response to fungal infection in several ways. First, we identified and classified proteins and cellular pathways in host cells that displayed increased or decreased protein expression or phosphorylation following infection (Tables 1, S1, S2, S3, and S4; Figure S1A). This analysis showed that proteins representing a broad array of biological processes, cellular components, and molecular functions were differentially phosphorylated during infection (Tables 1, S2, and S4). Second, we compared the set of host proteins that were differentially phosphorylated in response to Cn infection to corresponding sets of proteins from divergent bacterial or viral pathogens. This analysis identified proteins that were responsive to several infectious agents (Figure S1B). Finally, motif (Figure S1C), STRING (Figures S2C and S2D), and KEGG pathway analyses (Figure 2) revealed that proteins in the mTOR, STK11/LKB1, and AMPK-AIC signaling networks were differentially phosphorylated in response to Cn infecton (Figures S2C and S2D). These observations led us to test the hypothesis that host AMPK-AIC network proteins confer susceptibility to fungal infection.

Validation of Phosphoproteomic Findings using In Vitro, Ex Vivo, and In Vivo Systems

We used in vitro, ex vivo, and in vivo systems to test the hypothesis that Cn infection activates the host AMPK-AIC network. First, western blot (Figures 3A–I and S3A) and phosphospecific flow cytometry analyses (PFC) (Figures 3J and S3B) showed that the phosphorylation of LKB1, AMPKα, ULK1, and RPS6 increased in RAW264.7 macrophages or MH-S alveolar macrophages (AMs) following infection with the pathogen. We also measured the phosphorylation of AMPKα in macrophages where the activities of LBK1, AMPKα,

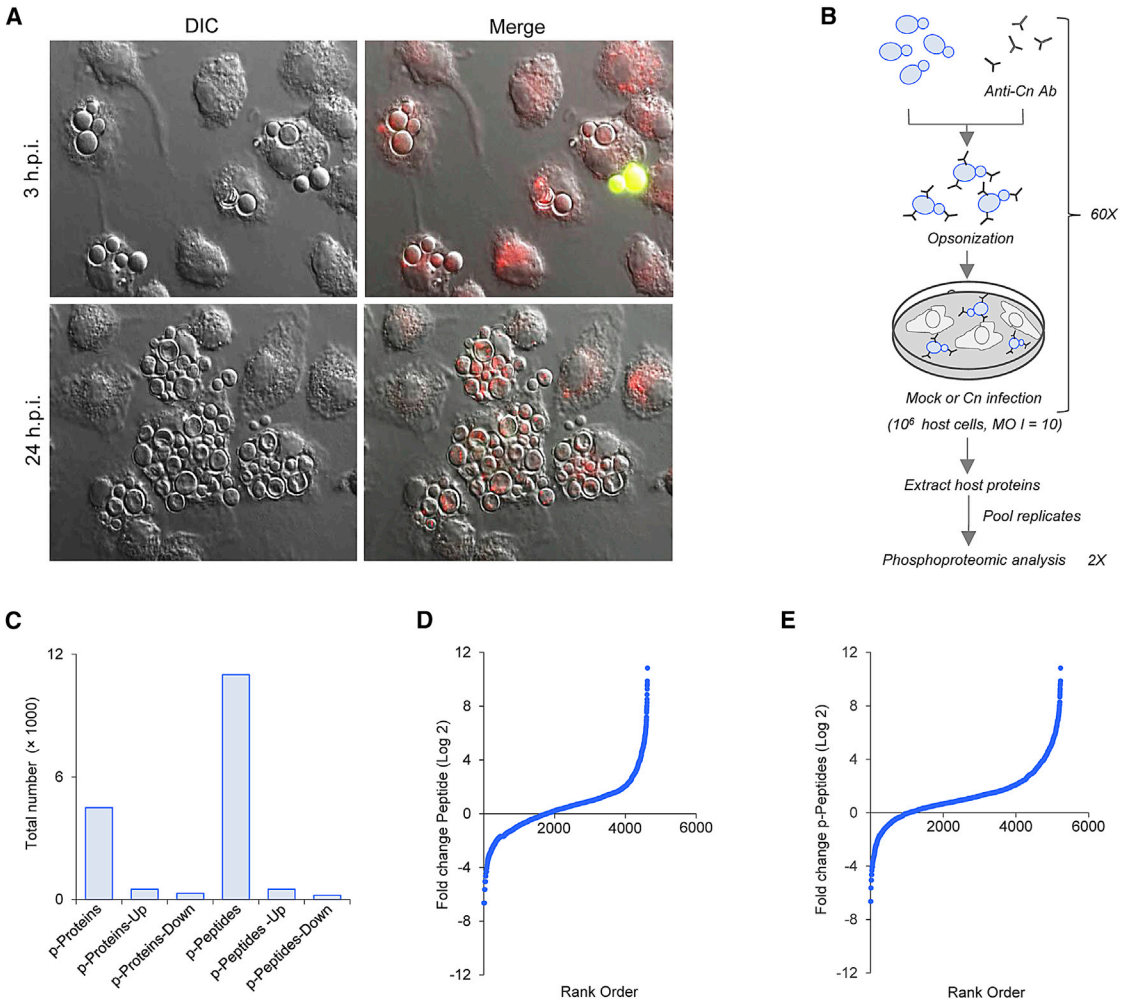

Figure 1. Cn Infection Induces Global Reprograming of the Host Phosphoproteome

(A) RAW264.7 macrophages were infected with antibody-opsonized Cn-dsRed. At 3 hr (top) or 24 hr (bottom) post-infection, the intracellular and extracellular Cn-dsRed populations were determined by staining unpermeabilized infected host cells. The stained cells were then processed for DIC microscopy (left) or fluorescence imaging (right) (60×). The extracellular population of Cn-dsRed cells was stained green (right).

(B) Workflow for phosphoproteomic analysis of mock- or Cn-infected RAW264.7 cells (n = 60).

(C–E) Total numbers (C) of phosphoproteins and phospho-peptides identified by LC-MS/MS analysis. The numbers of phosphoproteins and phosphopeptides that displayed 1.5-fold or greater enhancement (up) or reduction (down) in their levels of phosphorylation are also shown. Log_2 curve of the peptide (D) or phosphopeptide (E) abundance ratios for Cn-infected cells versus mock-infected controls. Abbreviations are as follows: Cn, *Cryptococcus neoformans*; h.p.i., hr post-infection; MOI, multiplicity of infection; DIC, differential interference contrast; LC-MS/MS, liquid chromatography-tandem mass spectrometry. See also Figures S1, S2, and S7 and Tables S1 and S2.

ULK1, FIP200, or ATG13 had been disrupted, depleted, or pharmacologically manipulated (Figure S3C). We observed, as expected, that cells depleted of AIC components displayed striking defects in autophagy induction (Figures S3D, S4A, and S4B). More importantly, we found that host cells depleted of AIC components displayed reduced phosphorylation of host AMPKα at various times post-infection (Figure 3K). These data showed that the infection-dependent phosphorylation of AIC network components was dependent upon the activities of other proteins in the network.

To determine whether the phosphorylation of AIC proteins was also induced in an ex vivo model of infection, we inoculated murine splenocytes with Cn and then used PFC to analyze their phosphorylation at 30 min post-infection (mpi). We found that the phosphorylation of AMPKα and ULK1 was significantly enhanced following berberine treatment (positive control) or Cn infection (Figures 3L and 3M). To determine whether Cn infection also induced the phosphorylation of AMPKα and ULK1 in vivo, we inoculated mice with the pathogen via intraperitoneal injection, harvested splenocytes at 6 hr post-infection (hpi), and then subjected the recovered cells to PFC using antibodies directed against phosphorylated variants of AMPKα or ULK1. We again found that infected animals displayed enhanced phosphorylation of these proteins (when compared to uninfected controls) (Figures 3N and 3O). Results from our in vitro, ex vivo, and in vivo phosphorylation analyses therefore validated and extended findings from LC-MS/MS phosphoproteomic experiments.

Table 1. Over-represented Cn-Responsive KEGG Pathways in Infected Host Cells

Over-represented KEGG Pathways	Fold Enrichment	p Value
Spliceosome	4.9	3.80E-08
GnRH signaling pathway	3.9	1.90E-04
MAPK signaling pathway	2.5	2.00E-04
Nucleotide excision repair	5.9	3.20E-04
Neurotrophin signaling pathway	3.2	6.80E-04
mTOR signaling pathway	4.7	0.001
Fc gamma R-mediated phagocytosis	3.3	0.003
DNA replication	5.5	0.004
Gap junction	3.3	0.005
Long-term potentiation	3.6	0.006
Regulation of actin cytoskeleton	2.2	0.008
Oocyte meiosis	2.8	0.009
NOD-like receptor signaling pathway	3.6	0.01
Progesterone-mediated oocyte maturation	3	0.02
ErbB signaling pathway	2.9	0.02
Ribosome	2.9	0.02
Axon guidance	2.4	0.02
Renal cell carcinoma	3.2	0.02
Insulin signaling pathway	2.3	0.03
Cell cycle	2.2	0.05
Notch signaling pathway	3.2	0.07
T cell receptor signaling pathway	2.2	0.07
Vascular smooth muscle contraction	2.1	0.08
Cytosolic DNA-sensing pathway	2.9	0.09
Prion diseases	3.6	0.09

AMPK-AIC Network Activities Confer Susceptibility to Infection

We used several independent methods, including immunofluorescence microscopy assays (Qin et al., 2008), fluconazole protection assays (Qin et al., 2011), and flow cytometry assays (Nicola and Casadevall, 2012; Nicola et al., 2011), to analyze the phagocytosis or replication of the antibody-opsonized pathogen in murine RAW264.7, B6J2, or MH-S macrophages. These experiments revealed that host cells depleted of individual AIC components displayed resistance to phagocytosis (2 hpi) or intracellular replication (24 hpi) (Figures 4B–4H and S4C). Notably, resistance to intracellular replication was observed at various MOIs (i.e., MOI = 0.1, 1, 10), thereby indicating that this resistance phenotype displayed MOI-independence (Figure S4C).

To further explore the role of AMPK in conferring susceptibility to fungal phagocytosis or intracellular replication, we tested whether pharmacological manipulation of AMPK activity influenced these processes. To eliminate the possibility that the tested AMPK inhibitors or activators acted on pathogen targets, we washed drug-treated host cells extensively (to remove residual compounds from the culture dish) prior to coincubation with opsonized Cn (Figures S4D and S4E). We found that RAW264.7 cells treated with the AMPK activators AICAR, berberine (BBR) (Figure 4I), salicylate (Hawley et al., 2012), A769662 (Figure 4J), or rapamycin (Figure 4K) displayed increased susceptibility to pathogen internalization. However, host cells treated with compound C (CC), an AMPK inhibitor, displayed increased resistance to internalization (Figure 4I). Trypan blue exclusion analysis (Qin et al., 2011) ruled out the possibility that the observed resistance was an artifact of diminished host cell viability (Figure S4E). Urease activity, a fungal virulence determinant, was similar in controls and in cells treated for various lengths of time with compounds that modulate AMPK activity (Figure S4E). Capsule size was also unaffected by treatment with CC (Figure 4H).

Finally, we explored whether deletion or deficiency of host AMPK-AIC components disrupted phagocytosis. We found that the rate of phagocytosis of latex beads was similar in host cells depleted of ULK1, ATG13, or FIP200 and corresponding controls (Figure S4I). We also observed that *Coxiella burnetii* (RSA439, Nine Mile Phase II strain), an intracellular bacterial pathogen that traffics to and replicates within a lysosome-like compartment (van Schaik et al., 2013), displayed similar levels of internalization and intracellular replication in AMPKα-deficient and control bone-marrow-derived macrophages (BMDMs) (Figure S4J). These findings indicated that depletion or inactivation of host AMPK-AIC proteins neither caused general perturbations in the phagocytic machinery nor disrupted the internalization or replication of an intracellular bacterial pathogen.

AIC Components Are Recruited to Forming Phagosomes that Contain Cn

To test the hypothesis that host AMPK-AIC proteins influence CnCV biogenesis and maturation, we performed double-label immunofluorescence microscopy experiments in which the localization of pairwise combinations of AMPKα, ULK1, ATG13, FIP200, or ATG9 was determined in RAW264.7 cells following coincubation with Cn. We found that AIC proteins were recruited to forming phagosomes that contained the antibody-opsonized pathogen (Figure 5A). Macrophages that transiently expressed ATG9-GFP were also used to analyze the recruitment of AIC components to forming phagosomes and nascent CnCVs (Qin et al., 2011). Results from these experiments showed that ATG9-GFP was efficiently recruited to these structures in live cells containing the opsonized pathogen (Figure 5B). We extended these findings to primary BMDMs by demonstrating that AMPKα was recruited to forming phagosomes that contained the fungus (Figure 5C). Consistent with previous reports (Nicola et al., 2012) and analyses of archival data (Feldmesser et al., 2000), we failed to observe subcellular structures that were either demarcated or circumscribed by double-membrane vesicles (Figure 5D), a structural hallmark of canonical autophagosomes (Klionsky et al., 2016). To test the hypothesis that ATG9 recruitment to CnCVs was dependent upon the activities of AIC components, we used fluorescence microscopy to visualize the association of native ATG9 with CnCVs in macrophages that had been depleted of ULK1. We found that ATG9 recruitment was reduced in cells depleted of this protein (Figure 5E). Similar reductions were also observed in cells that had been depleted of AMPKα, ATG13, or FIP200 (Figure 5F). These observations were consistent with findings that macrophages individually depleted of AIC proteins displayed reduced internalization of the fungus (Figure 4). Taken together, our findings supported the hypothesis that the

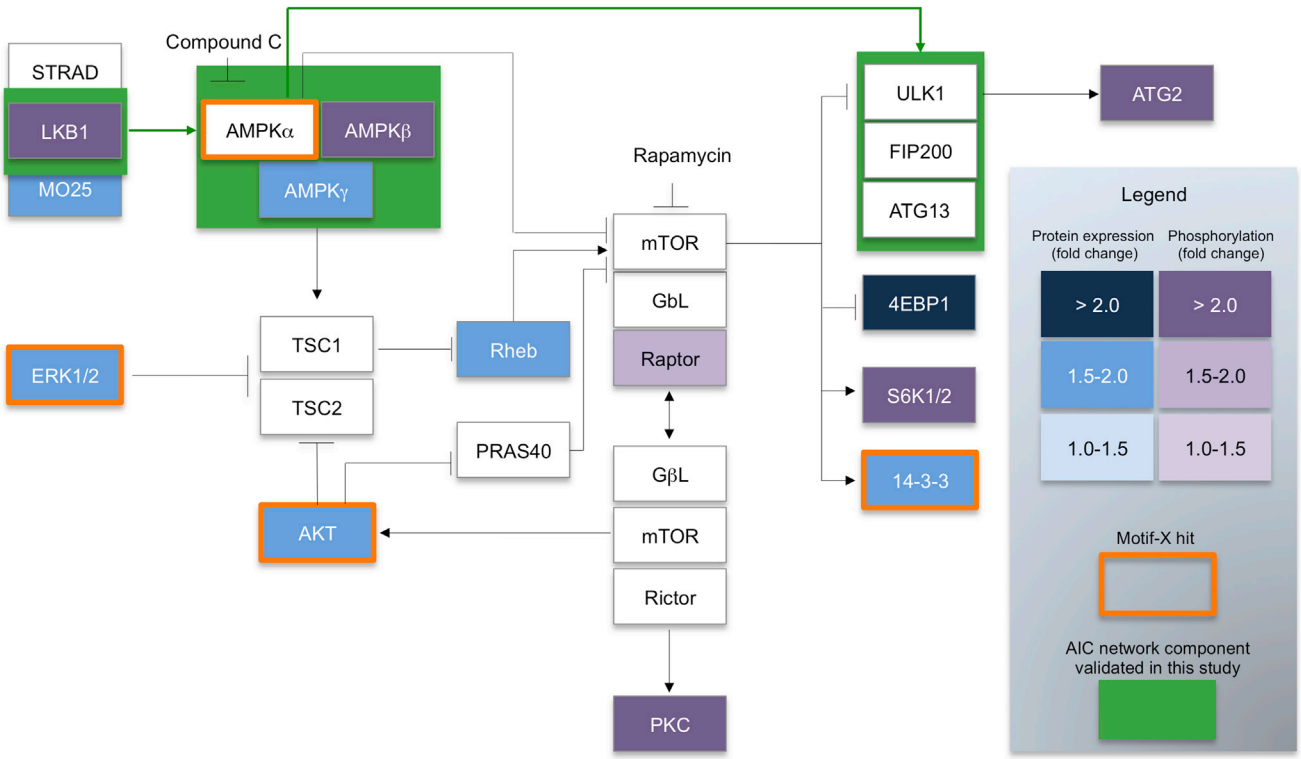

Figure 2. Cn Induces Activation of an AMPK Network

KEGG maps were generated to represent mTOR and AMPK network components that display responsiveness to Cn infection as revealed by phosphoproteomic or motif-X analyses. Abbreviations are as follows: Cn, *Cryptococcus neoformans*; KEGG, Kyoto Encyclopedia of Genes and Genomes. See also Figures S1 and S2 and Tables S1 and S2.

activities of individual AIC components control the internalization of Cn into host cells by being recruited to forming phagosomes to promote CnCV biogenesis.

AMPK Activity Confers Susceptibility to Cn Infection of Mice

To confirm and extend our pharmacological findings, we generated a tissue-specific *Prkaa1*$^{-/-}$ CKO mouse model (*Prkaa1*$^{f/f}$-*Lys2*$^{cre/-}$) in which the *Prkaa1* gene, which encodes AMPKα1, was selectively ablated from monocytes, macrophages, and granulocytes by the tissue-specific expression of Cre under control of the Lyz2 promoter (Figures 6A, S5A, and S5B). We then tested whether the phosphorylation AMPKα or ULK1 increased in response to infection in BMDMs or AMs from these (and corresponding littermate control) animals. At 24 hpi, AMPKα and ULK1 in BMDMs displayed increased (15-fold and 2.5-fold, respectively) phosphorylation on Thr172 and Ser555, respectively (Figure S5C). Phosphorylation of these residues induces the corresponding kinase activities (Egan et al., 2011; Momcilovic et al., 2006; Oakhill et al., 2011). BMDMs or AMs from *Prkaa1*$^{-/-}$ CKO mice, or BMDMs treated with CC, also displayed striking resistance to the phagocytosis and intracellular replication of the pathogen (Figures 6B, S5D, and S6A–S6D). Importantly, the resistance of *Prkaa1*$^{-/-}$ BMDMs to Cn intracellular parasitism was observed at differing MOIs (10, 1, 0.1), indicating that the resistance phenotype was not an artifact of the infectious dose used in these experiments (Figures S6E–S6F). Taken together, the data demonstrated that AMPKα conferred susceptibililty to Cn intracellular parasitism of primary cells in vitro.

Encouraged by our in vitro findings, we tested the hypothesis that AMPKα activity in macrophages conferred susceptibility to infection in vivo. First, in a pilot experiment, we treated mice with CC (or vehicle alone) (McCullough et al., 2005), and then, 24 hr post-treatment, we inoculated the treated animals with 1×10^7 CFU of Cn via intraperitoneal injection. We found that the drug-treated animals displayed striking resistance to fungal colonization of lung, liver, and spleen tissues at 6 hpi (Figure 6C). To extend these findings, we further characterized *Prkaa1*$^{-/-}$ CKO animals and then tested their susceptibility to Cn infection. Consistent with previous observations of animals in which AMPKα was ablated in all tissues (Jørgensen et al., 2004; Mounier et al., 2013), we found that the CKO animals had normal organ morphologies, fertility, growth, and development (data not shown). In addition, we observed that the percentages of $CD19^+$ B, $CD4^+$ and $CD8^+$ T, and $CD11b^+$ monocyte cells in splenocytes were similar in *Prkaa1*$^{-/-}$ CKO and control animals (*Prkaa1*$^{f/f}$-*Lys2*$^{-/-}$), which did not express Cre and therefore had the Prkaa1 gene intact (Figures 6D and 6E).

We infected control and *Prkaa1*$^{-/-}$ CKO mice with Cn via pulmonary installation to mimic the natural route of infection and then assessed pathogen burden, dissemination, and tissue pathology in infected control and CKO animals at 6 hpi and 14 days post-infection (dpi). These time points were selected for their utility in elucidating events associated with

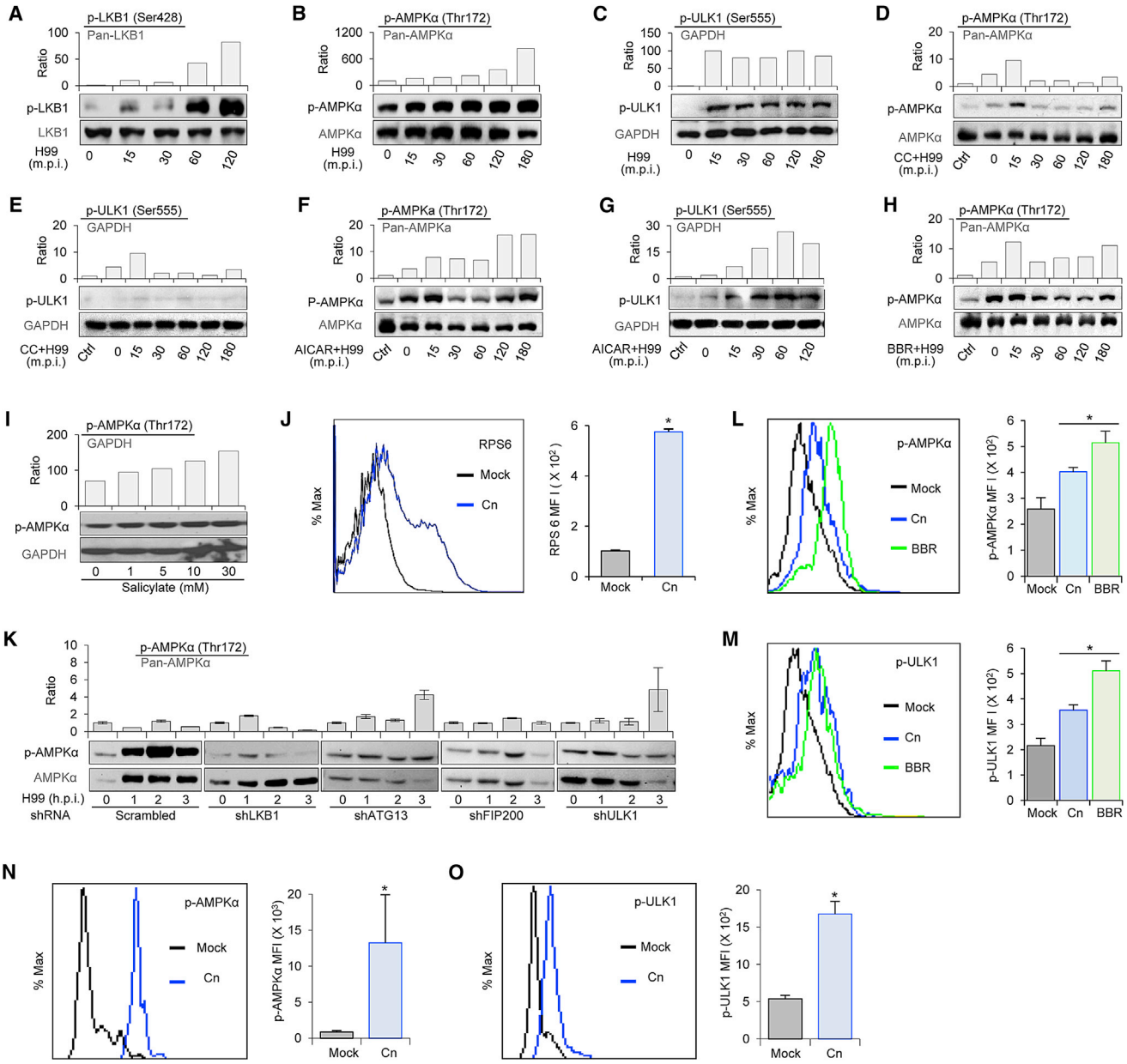

Figure 3. Cn Infection Induces Activation of AIC Signaling in Host Cells

(A–C) Western blot (bottom) and ImageJ-based quantification (top) of host LKB1 (A), AMPKα (B), and ULK1 (C) phosphorylation during a time course of Cn infection of RAW 264.7 cells.

(D–I) Effects of compounds that modulate AMPKα activity on Cn-induced phosphorylation of host AMPKα and ULK1. Western blot (bottom) and quantification (top) was performed on cell lysates to detect and quantify the phosphorylation of AMPKα (Thr172) and/or ULK1 (Ser555). Shown are (D) CC, AMPKα; (E) CC, p-ULK1; (F) AICAR, p-AMPKα; (G) AICAR, p-ULK1; (H) BBR, p-AMPKα; and (I) Salicylate, p-AMPKα.

(J) Activation of host ribosomal protein S6 (Ser235/236) by Cn infection. RAW 264.7 cells were infected with Cn. At 3 hpi, the infected cells were processed for flow cytometry to assess RPS6 (Ser235/236) activation. A representative overlay histogram and the average and SD of the mean flourescence intensities (MFI) are shown (n = 4). Black and blue histograms represent mock-infected and Cn-infected groups, respectively.

(K) Cn-induced phosphorylation of AMPKα is dependent upon LKB1 and AIC components. RAW264.7 macrophages depleted of LKB1, ATG13, FIP200, or ULK1 were infected with Cn. At the indicated time points post-infection, lysates from the infected cells were analyzed by western blot using p-AMPK (Thr172) or pan-AMPK antibodies. Results from one representative experiment (n = 5) are shown.

(L and M) CD11b$^+$ cells from splenocytes of WT mice were mock-infected or infected ex vivo with Cn for 30 min. The levels of phosphorylation of AMPKα (L) or ULK1 (M) were then determined by flow cytometry using antibodies directed against p-AMPKα (Thr172) or p-ULK1 (Ser555), respectively. Black, blue, and green histograms represent mock-infected, Cn-infected, and AMPK activator berberine (BBR)-treated groups (n = 4 per group), respectively.

(N and O) In vivo activation of AMPKα (N) or ULK1 (O) in CD11b$^+$ cells from the spleens of mock-infected or infected WT mice at 6 hpi was determined by phospoflow cytometry using antibodies against p-AMPKα1 (Thr172) or p-ULK1 (Ser555), respectively. Representative overlay histograms and average MFIs

(legend continued on next page)

internalization of the pathogen into host cells (6 hpi) and the intracellular replication, tissue dissemination and colonization of the pathogen (14 dpi), respectively (Rivera et al., 2002). We found that the *Prkaa1*$^{-/-}$ CKO animals displayed significant reductions in fungal load at 6 hpi (Figure 6f) and 14 dpi (Figure 6G) compared to littermate controls. To test the hypothesis that AMPKα activity in myeloid cells contributed to the observed differences in fungal tissue colonization, we infected control and CKO mice with Cn, harvested CD11b^{+} cells from spleens at 14 dpi, and then compared the fungal burden in the corresponding cell populations. We found that CD11b^{+} myeloid cells from *Prkaa1*$^{-/-}$ CKO animals harbored fewer Cn than controls (Figure 6H), thereby indicating that differential interactions between CD11b^{+} cells and Cn contributed to the resistance to intracellular parasitism observed in Prkaa1 CKO mice.

To test the hypothesis that alterations in the production of specific cytokines by CKO animals or *Prkaa1*$^{-/-}$ host cells significantly influenced fungal burden, we examined the accumulation of several key cytokines (IFN-γ, IL-6, and/or TNFα) in tissues or BMDMs at various times post-infection (Davis et al., 2013). IL-6 production by LPS-stimulated BMDMs was statistically indistinguishable in control and *Prkaa1*$^{-/-}$ CKO animals (data not shown). In addition, statistically significant differences in the production of TNFα or IL-6 by Cn-infected BMDMs were not observed at 24 hpi (Figure S6E; data not shown). Finally, differences in the abundance of key inflammatory mediators (IFN-γ, IL-6, and/or TNFα) in the spleen or lung of infected *Prkaa1*$^{-/-}$ CKO mice and controls were not observed at 14 dpi (Figure S6H; data not shown). Taken together, these findings support the hypothesis that alterations in these cytokine activities at the examined times did not influence fungal burden.

Histology of the lungs of infected animals revealed that the reduced fungal burden in the tissues of *Prkaa1*$^{-/-}$ CKO animals was associated with reductions in the severity of histopathologic changes at 14 dpi (Figure 6I). Approximately 90% of the alveolar spaces in the control animals were affected, while only ~70% of the alveolar spaces in the lungs of *Prkaa1*$^{-/-}$ CKO animals were involved. The interstitial spaces of the alveolar septa were expanded with fibrin and inflammatory cells comprised primarily of macrophages and lesser granulocytes. In the lungs from controls, the inflammation was moderate to marked, and the interstitium of the alveolar septa were expanded up to six layers thick. However, the inflammation in the lung from CKO animals was mild to moderate and alveolar septal interstitia were only two to three cell layers thick. The number of inflammatory foci was higher in the liver of controls (0.47 foci per high-powered field, hpf) than in *Prkaa1*$^{-/-}$ CKO animals (0.1 foci per hpf). In addition, the sizes of inflammatory foci in the liver from controls were larger than CKO animals (diameters of 300 μM and 150 μM, respectively). Therefore, *Prkaa1*$^{-/-}$ CKO animals displayed reduced severity of histopathologic changes at 14 dpi, supporting the conclusion that AMPKα activity confers susceptibility to Cn infection and promotes disease.

DISCUSSION

This study provides a global analysis of protein phosphorylation events in host cells infected with a fungal pathogen. Our analysis revealed that the infection of macrophages with antibody-opsonized Cn leads to global reprogramming of host signaling pathways. The scope of reprogramming was broad and included pathways that control the metabolism, signaling and cytoskeletal architecture of host cells. These findings extend previous studies in which the global analysis of the transcriptional response to Cn infection demonstrated reprogramming of host transcriptional circuitry (Chen et al., 2015; Liu et al., 2014).

We found that proteins in the host AMPK-AIC signaling network are differentially phosphorylated in response to fungal infection. The consequences of the phosphorylation of Ser428, Thr172, and Ser555 on the activities of LKB1, AMPKα, and ULK1, respectively, have been described (Xie et al., 2006b; Momcilovic et al., 2006; Oakhill et al., 2011; Egan et al., 2011). Morevoer, the impact of the phosphorylation of these residues on autophagy has been demonstrated (for reviews, see Alers et al., 2012 and Roach, 2011). Finally, the compounds used in our experiments regulate the phosphorylation of specific residues in target proteins (Zhou et al., 2001). Therefore, our findings revealed the functional importance of specific phosphorylation events on AMPK-AIC network proteins during fungal infection.

The intracellular lifestyle of Cn is pivotal for pathogen colonization, dissemination, and disease progression (Johnston and May, 2013) as well as for establishment of latent infection (Saha et al., 2007). Our findings indicate that the phosphorylation-dependent activation of host proteins in the AMPK-AIC signaling network confers susceptibility to fungal internalization and intracellular replication. As such, this work is consistent with previous studies that suggested roles for some host ATG proteins (e.g., ATG9) in regulating phagocytosis (Mehta et al., 2014; Qin et al., 2011; Sanjuan et al., 2007). However, other studies showed that host ATG5 activity did not confer enhanced susceptibility to fungal tissue colonization in vivo (Nicola et al., 2012). Therefore, our findings suggest that an ATG5-independent pathway contributes to susceptibility to fungal infection.

Several reports have investigated the complex relationship between autophagy and inflammatory responses. Based on these findings, it seems unlikely that the reduced inflammatory pathology observed in infected *Prkaa1*$^{-/-}$ CKO animals emerges solely as a consequence of their reduced autophagic potential. For example, several studies have shown that mice harboring deficiencies in ATG5 present increased lung inflammation when compared to controls (Qu et al., 2007; Suzuki et al., 2016). The same pattern of increased inflammatory responses was observed in the skin of mice harboring a deletion of *Fip200* (Wei et al., 2009). In our work, we showed that uninfected *Prkaa1*$^{-/-}$ CKO mice displayed normal morphology and the same percentage of monocytic cells as controls. However, infected CKO mice displayed reductions in fungal load. Furthermore, these animals presented less prominent inflammatory

(with SD) are displayed (n = 5 per group). Black and blue histograms represent mock-infected and Cn-infected groups, respectively. Images were from one representative experiment (n = 3). Abbreviations are as follows: AICAR, 5-Aminoimidazole-4-carboxamide ribonucleotide; BBR, berberine; CC, compound C; Cn, *Cryptococcus neoformans*; MFI, mean fluorescence intensity; MOI, multiplicity of infection; m.p.i., min post-infection; PBS, phosphate-buffered saline; SD, standard deviation; WB, western blot; WT, wild-type. See also, Figures S3, S4, and S7.

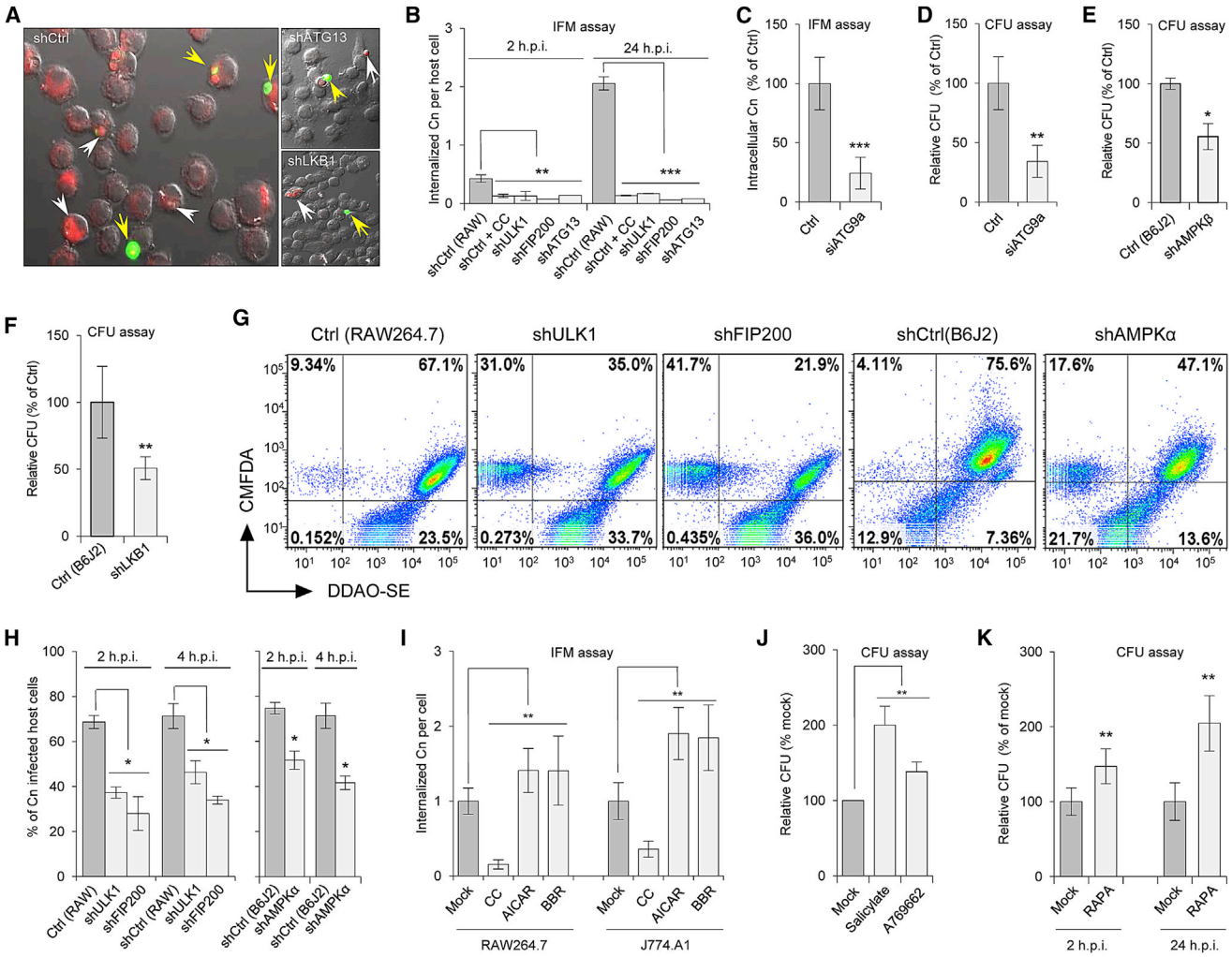

Figure 4. Depletion or Inhibition of Host AIC Components Disrupted the Intracellular Lifestyle of Cn

(A) ATG13-depleted or LKB1-depleted host cells show resistance to Cn infection. Scrambled control, ATG13-depleted, or LKB1-depleted RAW264.7 cells were infected with Cn-dsRed. At 2 hpi, the extracellular Cn population was visualized by immunofluorescence staining of unpermeabilized cells. White arrows indicate unstained intracellular Cn-dsRed cells. Yellow arrows indicate extracellular Cn-dsRed cells.

(B–H) shRNA-mediated depletion or pharmacological inactivation of host AMPKα, AMPKβ, ATG13, FIP200, LKB1, ULK1, or ATG9 reduced the phagocytosis of antibody-opsonized Cn by RAW264.7 or B6J2 macrophages, as indicated. Phagocytosis of Cn was measured using immunofluorescence microscopy (IFM) analysis to enumerate the number of internalized Cn per host cell at 2 or 24 hpi (B and C), by fluconazole protection colony formation unit (CFU) analysis to determine relative internalization (D–F) (Qin et al., 2011), or by flow cytometry (G–H) (Nicola et al., 2011). (B) IFM assay data from experiments in which AMPKα, ULK1, FIP200, or ATG13 were inactivated or depleted from host cells. (C) IFM assay data from experiments in which ATG9 was depleted from host cells. (D) CFU assay data from experiments in which ATG9 was depleted from host cells. (E) CFU assay data from experiments in which AMPKβ was depleted from host cells. (F) CFU assay data from experiments in which LKB1 was depleted from host cells. Representative dot plots (G) and histograms (H) of flow cytometry findings for the indicated times post-infection are shown. Data in B–F and H represent the mean and SD from six independent experiments. *, significance at $p < 0.05$; **, significance at $p < 0.01$, ***, significance at $p < 0.001$.

(I–K) Pretreatment of host cells (I) with AMPKα inhibitor compound C (CC, 20 μM) or activators AICAR (20 μM), BBR (20 μM), (J) salicylate (10 mM), A769662 (100 μm), or (K) rapamycin (10 μm) significantly decreased or increased, respectively, Cn phagocytosis. Data represent the mean and SD from six independent experiments. *, significance at $p < 0.05$; **, significance at $p < 0.01$. Abbreviations are as follows: AICAR, 5-aminoimidazole-4-carboxamide ribonucleotide; BBR, berberine; CC, compound C; CMFDA, 5-chloromethylfluorescein diacetate; Cn, *Cryptococcus neoformans*; Ctrl, control; DDAO-SE, 9-H-(1,3-dichloro-9,9-dimethylacridin-2-one-7-yl)-succinimidyl ester; MOI, multiplicity of infection; h.p.i., hr post-infection; RAPA, rapamycin; SD, standard deviation; WT, wild-type. See also Figures S3, S4, and S7.

infiltrates in liver and lung than controls. Thus, our findings suggest that the level of fungal burden is positively correlated with inflammatory alterations.

Our data indicate that Cn-induced phosphorylation of host LKB1 drives the downstream phosphorylation or engagement of AIC proteins, including FIP200, ATG13, and ULK1 (Figure S7). In classical autophagy, the activities of these proteins play crucial roles in recruiting membrane for the biogenesis of autophagosomes. It is tempting to speculate that these proteins play similar roles during Cn internalization, intracellular

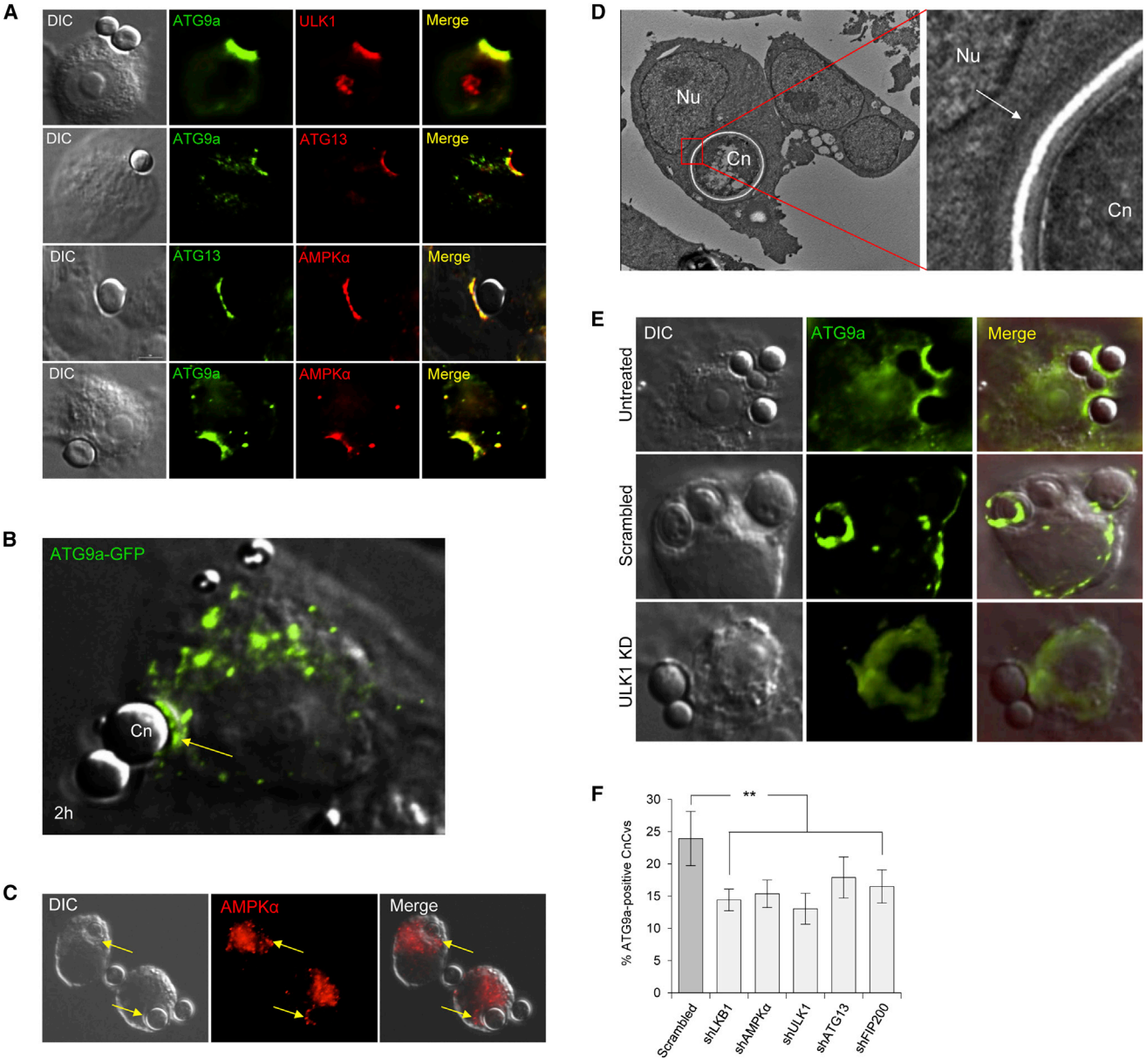

Figure 5. AIC and AIC Regulatory Components are Coordinately Recruited to Forming Phagosomes and Nascent CnCVs

(A) Immunofluoscence microscopy was used to analyze the recruitment and colocalization of AIC and AIC regulatory proteins (host AMPKα, ULK1, ATG13, FIP200, and ATG9) on forming phagosomes and nascent CnCVs in RAW264.7 macrophages at 2 hpi.

(B) Representative live-cell fluorescence microscopy image of ATG9a-GFP recruitment to forming phagosomes containing Cn. The yellow arrows indicate regions of notable ATG9a-GFP recruitment.

(C) Representative immunofluorescence micrograph demonstrating the recruitment of host AMPKα to forming phagosomes that contain Cn. The yellow arrows indicate regions of notable AMPKα recruitment.

(D) Representative transmission electron micrograph of a Cn-infected RAW264.7 macrophage showing a CnCV circumscribed by a single host membrane.

(E) Immunofluorescence micrographs depicted the diminished ATG9a recruitment to nascent CnCVs in host cells depleted of ULK1 compared to nondepleted controls.

(F) Quantification of the amount of ATG9a recruitment to forming pathogen-containing phagosomes or nascent CnCVs in RAW264.7 macrophages depleted of the indicated AIC proteins. Data represent the means ± SDs from three independent experiments. **, significance at $p < 0.01$. Scale bar represents 5 μM. Abbreviations are as follows: Cn, *Cryptococcus neoformans*; CnCV, *Cryptococcus neoformans*-containing vacuole; Ctrl, control. See also Figure S7.

trafficking, or replication. Cn is notable for its large size (compared to bacterial or viral pathogens), a morphological feature that is further exaggerated by its expansive capsule. These physical features may place unusual demands on host membrane trafficking systems that regulate pathogen internalization. Thus, AMPK-AIC network activity may be subverted by the pathogen to address this demand (Case et al., 2016), which, in turn, may contribute to the massive reprograming of host

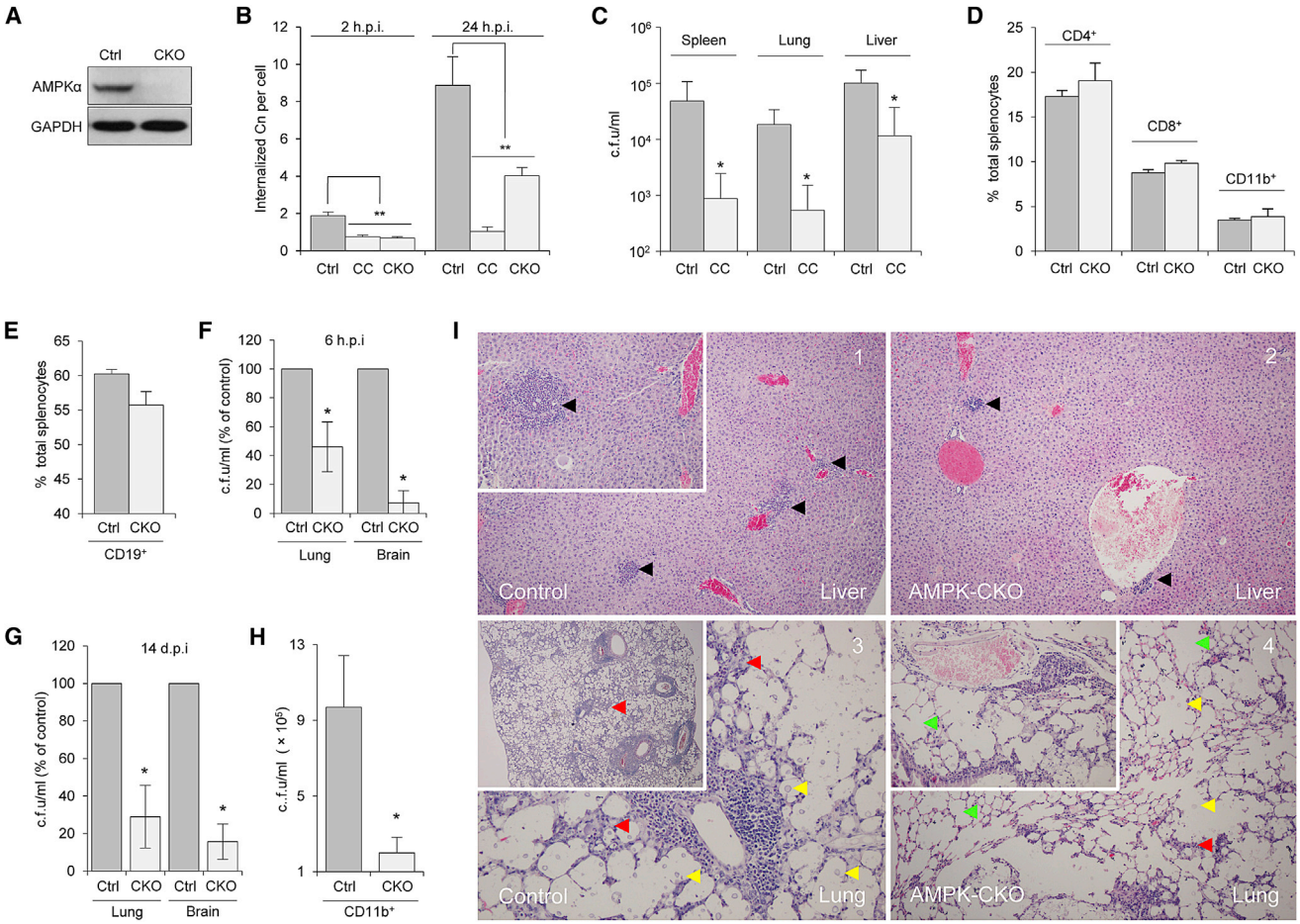

Figure 6. Host AMPKα Activity Confers Susceptibility to Cn Infection of Primary Cells and Mice

(A) Western blot analysis of AMPKα protein expression in control (Ctrl) and *Prkaa1*$^{-/-}$ CKO mice harboring deletions in the gene encoding AMPKα.

(B) Murine BMDMs pretreated with CC (20 μM) displayed resistance to pathogen internalization. In addition, *Prkaa1*$^{-/-}$ (CKO) BMDMs displayed striking resistance to phagocytosis (2 hpi) or intracellular replication (24 hpi) of the pathogen compared to *Prkaa1*$^{+/+}$ controls.

(C) Treatment of mice with the AMPKα inhibitor compound C (CC) reduced Cn tissue burden in infected animals. Fungal burden in the indicated tissues was analyzed at 6 hpi by plating homogenized tissue dilutions on solid medium (YPD-agar). Data represent CFU/mL, mean ± SD from three replicate experiments, each with five mice/group. *, significance at $p < 0.05$.

(D and E) Immunological characterization of Prkaa1 CKO mice. Splenocytes from control (Ctrl) and CKO mice were stained with fluorescently labeled antibodies against CD4, CD8 CD11b, and CD19 to assess the percentage of T cell subsets and CD11b^{+} myeloid cells (D) and B cells (E), respectively, in the spleen of CKO and control mice by flow cytometry. Data represent mean ± SD of percentage of indicated cells in total splenocytes from five mice.

(F and G) Cn burden in the tissues of Cn-infected *Prkaa1*$^{-/-}$ CKO or littermate control mice at 6 hpi or 14 dpi. Mice from each group were infected with 10^5 Cn via intrapulmonary instillation, and the fungal burden in the indicated tissues was determined at 6 hpi (F) or 14 DPI (G). Data represent the mean percentage of tissue fungal burden in the control. Data were from three independent experiments with five mice per group in each experiment. *, significance at $p < 0.05$.

(H) Cn burden in CD11b^{+} myeloid cells isolated by magnetic separation from splenocytes of Cn-infected (i.p.) CKO or control mice at 14 DPI. Data represent the mean ± SD. CFU/mL from five mice. *, significance at $p < 0.05$.

(I) Histopathology of representative hematoxylin and eosin (H&E) stained sections of tissues (liver, 1 and 2; lung, 3 and 4) from Cn-infected control (1 and 3) or CKO (2 and 4) mice at 14 dpi. In the liver (1 and 2), inflammatory foci were randomly distributed (black arrowheads) but were more numerous and larger in control animals. Inset in 1 shows detail of an inflammatory focus. In the images of lung tissue (3 and 4), the yellow arrowheads point to fungal organisms within the alveolar spaces. While most alveoli in control mice contained fungi, the alveoli of *Prkaa1*$^{-/-}$ CKO mice were often clear of pathogen (green arrowheads). The red arrowheads demonstrate that the interstitium of the lung was infiltrated with inflammatory cells and thicker in control animals. Inset in 3 shows a low-magnification (4×) image of inflammed pulmonary tissue. Inset in 4 shows a high-magnification image of pulmonary tissue with alveolar spaces clear of fungi. Abbreviations are as follows: CFU, colony-forming units; CKO, conditional knockout; Ctrl, control; Cn, *Cryptococcus neoformans*; h.p.i., hr post-infection; d.p.i., days post-infection; SD, standard deviation. See also Figures S5–S7.

signaling networks that accompanies infection. Future work will be directed toward further interrogating this possibility.

Several aspects of our findings provide opportunities for further investigation. First, the phosphoproteomic profiles reported here were generated from host cells infected with antibody-opsonized Cn. A limitation of our experimental design is that opsonin-independent responses could not be distinguished from their opsonin-dependent counterparts. Morever, the proteome represents the host response to infection at 2 hpi. It is likely, however, that different sets of proteins would be differentially

phosphorylated at different time points. Finally, the advantages and limitations of the proteomics approaches employed in this study have been reported (Asara et al., 2008; Merl et al., 2012; Wasinger et al., 2013). Future work that exploits alternative proteomic approaches will complement this study.

STAR★METHODS

Detailed methods are provided in the online version of this paper and include the following:

- KEY RESOURCES TABLE
- CONTACT FOR REAGENT AND RESOURCE SHARING
- EXPERIMENTAL MODEL AND SUBJECT DETAILS
  - Generation, Genotyping, and Characterization of Prkaa1$^{f/f}$-Lys2$^{cre/-}$ Mice
  - Bone-Marrow-Derived Macrophage and Alveolar Macrophage Harvest and Cultivation
- METHOD DETAILS
  - *Cryptococcus* Strains, Immortalized Cell Culture, *Cryptococcus* Infection, and CFU Assay
  - Infection of Host Cells with Ab-opsonized or Unopsonized Cn
  - Sample Preparation for Proteomic Analyses
  - Sample Digestion
  - Phosphopeptide Enrichment
  - NanoLC MS/MS Analyses
  - Database Searching and Analyses
  - Bioinformatic Analyses
  - Drug Treatments
  - Retrovirus Infection and shRNA-Catalyzed Depletion of Host Proteins
  - Microscopy
  - Immunoblotting Analysis
  - Ex Vivo or In Vivo Stimulation and Phosphorylation Analyses
  - Phagocytosis Assays
  - Animal Infections with Cn and Tissue Analysis
  - Infection of Host Cells with *Coxiella burnetii*
- QUANTIFICATION AND STATISTICAL ANALYSIS
- DATA AND SOFTWARE AVAILABILITY

SUPPLEMENTAL INFORMATION

Supplemental Information includes seven figures and six tables and can be found with this article online at http://dx.doi.org/10.1016/j.chom.2017.04.008.

AUTHOR CONTRIBUTIONS

Experiments were designed and performed as follows: phosphoproteomic analysis by A.P., S.L.D., P.d.F., and W.K.R.; bioinformatic analyses by R.G., S.-H.S., and X.Q.; in vitro infection and imaging by A.P., S.L.D., X.F., W.J.B., and Q.M.Q.; knockdown cell lines and flow cytometry by A.P., M.K., F.L., G.M.R., R.C.A., and S.P.C.; *Coxiella* by E.D.C., E.J.v.S., and J.E.S.; animal experiments by A.P., T.S., L.F.d.C., K.S.K., and P.d.F.; and tissue pathology by O.K., A.A., and G.G. The overall project was designed by A.R.-F., W.K.R., T.A.F., and P.d.F. The manuscript was written by S.-H.S., X.Q., W.K.R., T.A.F., and P.d.F.

ACKNOWLEDGMENTS

We thank Dr. J. Jill Suttles (University of Louisville School of Medicine) for *B6J2* macrophages expressing dominant negative and corresponding control variants of AMPK, Dr. Arturo Casadevall (Albert Einstein College of Medicine) for 18B7 anticryptococcal antibodies, Dr. Noboru Mizushima (University of Tokyo) for ATG9a-GFP expression plasmid, and Drs. Katherine Watson and Jane Miller (TAMHSC Cell Analysis Facility) for assistance with the flow cytometry. This research was supported by a Texas A&M University – Weizmann Institute of Science grant to T.A.F. and P.d.F.; Texas A&M University – CAPES awards to L.F.C. and P.d.F.; grant awards NIH 1R01 AI48496-01A1, USDA/CSREES-NRICGP 99-35204-7550, and NIH 1U54AI057156-0100 to T.AF.; grant NIH AI110642 to RCA; grant awards NIH R01AI090142-01A1 and DoD HDTRA1-13-1-0003 to J.E.S.; grants from NIH (R01DK074738), CST*R, TAM Genomics, and CTEHR to K.S.K.; and grant awards from NSFC (81371773) and Jilin University (4305050102 and 450060491563) to Q.M.Q. In addition, X.Q. is partially supported by NSF awards CCF-1447235 and CCF-1553281. Any opinions, findings, conclusions or recommendations expressed in this material are those of the authors and do not necessarily reflect the views of the funding agencies.

Received: August 22, 2016
Revised: March 12, 2017
Accepted: April 24, 2017
Published: May 10, 2017

SUPPORTING CITATIONS

The following references appear in the Supplemental Information: Chaki et al. (2013); Ganley et al. (2009); Imami et al. (2013).

REFERENCES

Alers, S., Löffler, A.S., Wesselborg, S., and Stork, B. (2012). Role of AMPK-mTOR-Ulk1/2 in the regulation of autophagy: cross talk, shortcuts, and feedbacks. Mol. Cell. Biol. *32*, 2–11.

Asara, J.M., Christofk, H.R., Freimark, L.M., and Cantley, L.C. (2008). A label-free quantification method by MS/MS TIC compared to SILAC and spectral counting in a proteomics screen. Proteomics *8*, 994–999.

Bozzola, J.J. (2007). Conventional specimen preparation techniques for transmission electron microscopy of cultured cells. Methods Mol. Biol. *369*, 1–18.

Case, E.D., Smith, J.A., Ficht, T.A., Samuel, J.E., and de Figueiredo, P. (2016). Space: a final frontier for vacuolar pathogens. Traffic *17*, 461–474.

Chaki, S.P., Barhoumi, R., Berginski, M.E., Sreenivasappa, H., Trache, A., Gomez, S.M., and Rivera, G.M. (2013). Nck enables directional cell migration through the coordination of polarized membrane protrusion with adhesion dynamics. J. Cell Sci. *126*, 1637–1649.

Chen, S., Yan, H., Zhang, L., Kong, W., Sun, Y., Zhang, W., Chen, Y., and Deng, A. (2015). Cryptococcus neoformans infection and immune cell regulation in human monocytes. Cell. Physiol. Biochem. *37*, 537–547.

Chong, A., Wehrly, T.D., Nair, V., Fischer, E.R., Barker, J.R., Klose, K.E., and Celli, J. (2008). The early phagosomal stage of Francisella tularensis determines optimal phagosomal escape and Francisella pathogenicity island protein expression. Infect. Immun. *76*, 5488–5499.

Clausen, B.E., Burkhardt, C., Reith, W., Renkawitz, R., and Förster, I. (1999). Conditional gene targeting in macrophages and granulocytes using LysMcre mice. Transgenic Res. *8*, 265–277.

Davis, M.J., Tsang, T.M., Qiu, Y., Dayrit, J.K., Freij, J.B., Huffnagle, G.B., and Olszewski, M.A. (2013). Macrophage M1/M2 polarization dynamically adapts to changes in cytokine microenvironments in Cryptococcus neoformans infection. MBio *4*, e00264–13.

Egan, D.F., Shackelford, D.B., Mihaylova, M.M., Gelino, S., Kohnz, R.A., Mair, W., Vasquez, D.S., Joshi, A., Gwinn, D.M., Taylor, R., et al. (2011). Phosphorylation of ULK1 (hATG1) by AMP-activated protein kinase connects energy sensing to mitophagy. Science *331*, 456–461.

Feder, V., Kmetzsch, L., Staats, C.C., Vidal-Figueiredo, N., Ligabue-Braun, R., Carlini, C.R., and Vainstein, M.H. (2015). Cryptococcus gattii urease as a virulence factor and the relevance of enzymatic activity in cryptococcosis pathogenesis. FEBS J. *282*, 1406–1418.

Feldmesser, M., Kress, Y., Novikoff, P., and Casadevall, A. (2000). Cryptococcus neoformans is a facultative intracellular pathogen in murine pulmonary infection. Infect. Immun. *68*, 4225–4237.

Ganley, I.G., Lam, H., Wang, J., Ding, X., Chen, S., and Jiang, X. (2009). ULK1.ATG13.FIP200 complex mediates mTOR signaling and is essential for autophagy. J. Biol. Chem. *284*, 12297–12305.

Gomez, G., Pei, J., Mwangi, W., Adams, L.G., Rice-Ficht, A., and Ficht, T.A. (2013). Immunogenic and invasive properties of Brucella melitensis 16M outer membrane protein vaccine candidates identified via a reverse vaccinology approach. PLoS ONE *8*, e59751.

Hawley, S.A., Pan, D.A., Mustard, K.J., Ross, L., Bain, J., Edelman, A.M., Frenguelli, B.G., and Hardie, D.G. (2005). Calmodulin-dependent protein kinase kinase-beta is an alternative upstream kinase for AMP-activated protein kinase. Cell Metab. *2*, 9–19.

Hawley, S.A., Fullerton, M.D., Ross, F.A., Schertzer, J.D., Chevtzoff, C., Walker, K.J., Peggie, M.W., Zibrova, D., Green, K.A., Mustard, K.J., et al. (2012). The ancient drug salicylate directly activates AMP-activated protein kinase. Science *336*, 918–922.

Imami, K., Bhavsar, A.P., Yu, H., Brown, N.F., Rogers, L.D., Finlay, B.B., and Foster, L.J. (2013). Global impact of Salmonella pathogenicity island 2-secreted effectors on the host phosphoproteome. Mol. Cell. Proteomics *12*, 1632–1643.

Johnston, S.A., and May, R.C. (2013). Cryptococcus interactions with macrophages: evasion and manipulation of the phagosome by a fungal pathogen. Cell. Microbiol. *15*, 403–411.

Jørgensen, S.B., Viollet, B., Andreelli, F., Frøsig, C., Birk, J.B., Schjerling, P., Vaulont, S., Richter, E.A., and Wojtaszewski, J.F. (2004). Knockout of the alpha2 but not alpha1 5′-AMP-activated protein kinase isoform abolishes 5-aminoimidazole-4-carboxamide-1-beta-4-ribofuranosidebut not contraction-induced glucose uptake in skeletal muscle. J. Biol. Chem. *279*, 1070–1079.

Jung, C.H., Jun, C.B., Ro, S.H., Kim, Y.M., Otto, N.M., Cao, J., Kundu, M., and Kim, D.H. (2009). ULK-Atg13-FIP200 complexes mediate mTOR signaling to the autophagy machinery. Mol. Biol. Cell *20*, 1992–2003.

Kim, J.C., Crary, B., Chang, Y.C., Kwon-Chung, K.J., and Kim, K.J. (2012). Cryptococcus neoformans activates RhoGTPase proteins followed by protein kinase C, focal adhesion kinase, and ezrin to promote traversal across the blood-brain barrier. J. Biol. Chem. *287*, 36147–36157.

Klionsky, D.J., Abdelmohsen, K., Abe, A., Abedin, M.J., Abeliovich, H., Acevedo Arozena, A., Adachi, H., Adams, C.M., Adams, P.D., Adeli, K., et al. (2016). Guidelines for the use and interpretation of assays for monitoring autophagy (3rd edition). Autophagy *12*, 1–222.

Krutzik, P.O., and Nolan, G.P. (2003). Intracellular phospho-protein staining techniques for flow cytometry: monitoring single cell signaling events. Cytometry A *55*, 61–70.

Kwon-Chung, K.J., Wickes, B.L., Booth, J.L., Vishniac, H.S., and Bennett, J.E. (1987). Urease inhibition by EDTA in the two varieties of Cryptococcus neoformans. Infect. Immun. *55*, 1751–1754.

Liu, T.B., Subbian, S., Pan, W., Eugenin, E., Xie, J., and Xue, C. (2014). Cryptococcus inositol utilization modulates the host protective immune response during brain infection. Cell Commun. Signal. *12*, 51.

Mack, H.I., Zheng, B., Asara, J.M., and Thomas, S.M. (2012). AMPK-dependent phosphorylation of ULK1 regulates ATG9 localization. Autophagy *8*, 1197–1214.

Mao, K., and Klionsky, D.J. (2011). AMPK activates autophagy by phosphorylating ULK1. Circ. Res. *108*, 787–788.

McCullough, L.D., Zeng, Z., Li, H., Landree, L.E., McFadden, J., and Ronnett, G.V. (2005). Pharmacological inhibition of AMP-activated protein kinase provides neuroprotection in stroke. J. Biol. Chem. *280*, 20493–20502.

Mehta, P., Henault, J., Kolbeck, R., and Sanjuan, M.A. (2014). Noncanonical autophagy: one small step for LC3, one giant leap for immunity. Curr. Opin. Immunol. *26*, 69–75.

Merl, J., Ueffing, M., Hauck, S.M., and von Toerne, C. (2012). Direct comparison of MS-based label-free and SILAC quantitative proteome profiling strategies in primary retinal Müller cells. Proteomics *12*, 1902–1911.

Mi, H., Poudel, S., Muruganujan, A., Casagrande, J.T., and Thomas, P.D. (2016). PANTHER version 10: expanded protein families and functions, and analysis tools. Nucleic Acids Res. *44* (D1), D336–D342.

Momcilovic, M., Hong, S.P., and Carlson, M. (2006). Mammalian TAK1 activates Snf1 protein kinase in yeast and phosphorylates AMP-activated protein kinase in vitro. J. Biol. Chem. *281*, 25336–25343.

Mounier, R., Théret, M., Arnold, L., Cuvellier, S., Bultot, L., Göransson, O., Sanz, N., Ferry, A., Sakamoto, K., Foretz, M., et al. (2013). AMPKα1 regulates macrophage skewing at the time of resolution of inflammation during skeletal muscle regeneration. Cell Metab. *18*, 251–264.

Nakayasu, E.S., Tempel, R., Cambronne, X.A., Petyuk, V.A., Jones, M.B., Gritsenko, M.A., Monroe, M.E., Yang, F., Smith, R.D., Adkins, J.N., and Heffron, F. (2013). Comparative phosphoproteomics reveals components of host cell invasion and post-transcriptional regulation during Francisella infection. Mol. Cell. Proteomics *12*, 3297–3309.

Nicola, A.M., and Casadevall, A. (2012). In vitro measurement of phagocytosis and killing of Cryptococcus neoformans by macrophages. Methods Mol. Biol. *844*, 189–197.

Nicola, A.M., Robertson, E.J., Albuquerque, P., Derengowski, Lda.S., and Casadevall, A. (2011). Nonlytic exocytosis of Cryptococcus neoformans from macrophages occurs in vivo and is influenced by phagosomal pH. MBio *2*, e00167–11.

Nicola, A.M., Albuquerque, P., Martinez, L.R., Dal-Rosso, R.A., Saylor, C., De Jesus, M., Nosanchuk, J.D., and Casadevall, A. (2012). Macrophage autophagy in immunity to Cryptococcus neoformans and Candida albicans. Infect. Immun. *80*, 3065–3076.

Oakhill, J.S., Steel, R., Chen, Z.P., Scott, J.W., Ling, N., Tam, S., and Kemp, B.E. (2011). AMPK is a direct adenylate charge-regulated protein kinase. Science *332*, 1433–1435.

Qin, Q.M., Pei, J., Ancona, V., Shaw, B.D., Ficht, T.A., and de Figueiredo, P. (2008). RNAi screen of endoplasmic reticulum-associated host factors reveals a role for IRE1alpha in supporting Brucella replication. PLoS Pathog. *4*, e1000110.

Qin, Q.M., Luo, J., Lin, X., Pei, J., Li, L., Ficht, T.A., and de Figueiredo, P. (2011). Functional analysis of host factors that mediate the intracellular lifestyle of Cryptococcus neoformans. PLoS Pathog. *7*, e1002078.

Qu, X., Zou, Z., Sun, Q., Luby-Phelps, K., Cheng, P., Hogan, R.N., Gilpin, C., and Levine, B. (2007). Autophagy gene-dependent clearance of apoptotic cells during embryonic development. Cell *128*, 931–946.

Rivera, J., Mukherjee, J., Weiss, L.M., and Casadevall, A. (2002). Antibody efficacy in murine pulmonary Cryptococcus neoformans infection: a role for nitric oxide. J. Immunol. *168*, 3419–3427.

Roach, P.J. (2011). AMPK -> ULK1 -> autophagy. Mol. Cell. Biol. *31*, 3082–3084.

Rogers, L.D., Brown, N.F., Fang, Y., Pelech, S., and Foster, L.J. (2011). Phosphoproteomic analysis of Salmonella-infected cells identifies key kinase regulators and SopB-dependent host phosphorylation events. Sci. Signal. *4*, rs9.

Sabiiti, W., and May, R.C. (2012). Mechanisms of infection by the human fungal pathogen Cryptococcus neoformans. Future Microbiol. *7*, 1297–1313.

Sag, D., Carling, D., Stout, R.D., and Suttles, J. (2008). Adenosine 5′-monophosphate-activated protein kinase promotes macrophage polarization to an anti-inflammatory functional phenotype. J. Immunol. *181*, 8633–8641.

Saha, D.C., Goldman, D.L., Shao, X., Casadevall, A., Husain, S., Limaye, A.P., Lyon, M., Somani, J., Pursell, K., Pruett, T.L., and Singh, N. (2007). Serologic evidence for reactivation of cryptococcosis in solid-organ transplant recipients. Clin. Vaccine Immunol. *14*, 1550–1554.

Samuel, J.E., Frazier, M.E., and Mallavia, L.P. (1985). Correlation of plasmid type and disease caused by Coxiella burnetii. Infect. Immun. *49*, 775–779.

Sanjuan, M.A., Dillon, C.P., Tait, S.W., Moshiach, S., Dorsey, F., Connell, S., Komatsu, M., Tanaka, K., Cleveland, J.L., Withoff, S., and Green, D.R.

(2007). Toll-like receptor signalling in macrophages links the autophagy pathway to phagocytosis. Nature *450*, 1253–1257.

Schmutz, C., Ahrné, E., Kasper, C.A., Tschon, T., Sorg, I., Dreier, R.F., Schmidt, A., and Arrieumerlou, C. (2013). Systems-level overview of host protein phosphorylation during Shigella flexneri infection revealed by phosphoproteomics. Mol. Cell. Proteomics *12*, 2952–2968.

Sonnhammer, E.L., and Östlund, G. (2015). InParanoid 8: orthology analysis between 273 proteomes, mostly eukaryotic. Nucleic Acids Res. *43*, D234–D239.

Suzuki, Y., Maazi, H., Sankaranarayanan, I., Lam, J., Khoo, B., Soroosh, P., Barbers, R.G., James Ou, J.H., Jung, J.U., and Akbari, O. (2016). Lack of autophagy induces steroid-resistant airway inflammation. The Journal of allergy and clinical immunology *137*, 1382–1389 e1389.

Towbin, H., Staehelin, T., and Gordon, J. (1979). Electrophoretic transfer of proteins from polyacrylamide gels to nitrocellulose sheets: procedure and some applications. Proc. Natl. Acad. Sci. USA *76*, 4350–4354.

van Schaik, E.J., Chen, C., Mertens, K., Weber, M.M., and Samuel, J.E. (2013). Molecular pathogenesis of the obligate intracellular bacterium Coxiella burnetii. Nat. Rev. Microbiol. *11*, 561–573.

van Schaik, E.J., Case, E.D., Martinez, E., Bonazzi, M., and Samuel, J.E. (2017). The SCID mouse model for identifying virulence determinants in Coxiella burnetii. Front. Cell. Infect. Microbiol. *7*, 25.

Wasinger, V.C., Zeng, M., and Yau, Y. (2013). Current status and advances in quantitative proteomic mass spectrometry. Int. J. Proteomics *2013*, 180605.

Weerasekara, V.K., Panek, D.J., Broadbent, D.G., Mortenson, J.B., Mathis, A.D., Logan, G.N., Prince, J.T., Thomson, D.M., Thompson, J.W., and Andersen, J.L. (2014). Metabolic-stress-induced rearrangement of the 14-3-3ζ interactome promotes autophagy via a ULK1- and AMPK-regulated 14-3-3ζ interaction with phosphorylated Atg9. Mol. Cell. Biol. *34*, 4379–4388.

Wei, H., Gan, B., Wu, X., and Guan, J.L. (2009). Inactivation of FIP200 leads to inflammatory skin disorder, but not tumorigenesis, in conditional knock-out mouse models. J. Biol. Chem. *284*, 6004–6013.

Wojcechowskyj, J.A., Didigu, C.A., Lee, J.Y., Parrish, N.F., Sinha, R., Hahn, B.H., Bushman, F.D., Jensen, S.T., Seeholzer, S.H., and Doms, R.W. (2013). Quantitative phosphoproteomics reveals extensive cellular reprogramming during HIV-1 entry. Cell Host Microbe *13*, 613–623.

Woods, A., Johnstone, S.R., Dickerson, K., Leiper, F.C., Fryer, L.G., Neumann, D., Schlattner, U., Wallimann, T., Carlson, M., and Carling, D. (2003). LKB1 is the upstream kinase in the AMP-activated protein kinase cascade. Curr. Biol. *13*, 2004–2008.

Xie, M., Zhang, D., Dyck, J.R., Li, Y., Zhang, H., Morishima, M., Mann, D.L., Taffet, G.E., Baldini, A., Khoury, D.S., and Schneider, M.D. (2006a). A pivotal role for endogenous TGF-beta-activated kinase-1 in the LKB1/AMP-activated protein kinase energy-sensor pathway. Proc. Natl. Acad. Sci. USA *103*, 17378–17383.

Xie, Z., Dong, Y., Zhang, M., Cui, M.Z., Cohen, R.A., Riek, U., Neumann, D., Schlattner, U., and Zou, M.H. (2006b). Activation of protein kinase C zeta by peroxynitrite regulates LKB1-dependent AMP-activated protein kinase in cultured endothelial cells. J. Biol. Chem. *281*, 6366–6375.

Zhang, C., Wang, S.H., Lasbury, M.E., Tschang, D., Liao, C.P., Durant, P.J., and Lee, C.H. (2006). Toll-like receptor 2 mediates alveolar macrophage response to Pneumocystis murina. Infect. Immun. *74*, 1857–1864.

Zhou, G., Myers, R., Li, Y., Chen, Y., Shen, X., Fenyk-Melody, J., Wu, M., Ventre, J., Doebber, T., Fujii, N., et al. (2001). Role of AMP-activated protein kinase in mechanism of metformin action. J. Clin. Invest. *108*, 1167–1174.

STAR★METHODS

KEY RESOURCES TABLE

REAGENT or RESOURCE	SOURCE	IDENTIFIER
Antibodies		
Mouse anti-*C. neoformans* 18B7	Dr. Arturo Casadevall, (Albert Einstein College of Medicine of Yeshiva University, NY, USA)	N/A
Rabbit anti-pAMPKα (Thr 172)	Cell Signaling Technology, Inc. (Danver, MA USA)	Cat. #: 2535 RRID: AB_331250
Rabbit anti-AMPKα	Cell Signaling Technology, Inc. (Danver, MA USA)	Cat. #: 5831 RRID: AB_10622186
Rabbit-anti pULK1 (Ser 555)	Cell Signaling Technology, Inc. (Danver, MA USA)	Cat. #: 5869 RRID: AB_10707365
Rabbit anti-ULK1	Santa Cruz Biotechnology, Inc. (Dallas, TX USA)	Cat. #: sc-33182 RRID: AB_2214706
Rabbit anti-LC3	Santa Cruz Biotechnology, Inc. (Dallas, TX USA)	Cat. #: sc-134226 RRID: AB_2250051
Rabbit anti-GAPDH	Santa Cruz Biotechnology, Inc. (Dallas, TX USA)	Cat. #: sc-25778 RRID: AB_10167668
Rabbit anti-ATG13	Sigma-Aldrich, Inc. (St. Louis, MO USA)	Cat. #: SAB4200100 RRID: AB_10602787
Rabbit anti-FIP200	Proteintech Group, Inc. (Rosemont, IL USA)	Cat. #: 17250-1-AP RRID: AB_10666428
Rabbit anti-LKB1	Abgent, Inc. (San Diego, CA USA)	Cat. #: ASC10479
Rabbit anti-AMPKβ	Novus Biologicals, Inc. (Littleton, CO USA)	Cat. #: NBP1-87487 RRID: AB_11040810
Rabbit anti-pLKB1 (Ser428)	Abcam, Inc. (Cambridge, MA USA)	Cat. #: Ab63473 RRID: AB_1523886
Rabbit anti-pAMPK (Thr172)-PE	BIOSS, Inc. (Woburn, MA USA).	Cat. #: BS-4002RP
Rabbit anti-pATG1 (Ser556)-PE	BIOSS, Inc. (Woburn, MA USA)	Cat. #: ABIN746733
Rabbit anti-CD11b-APC	Thermo Fischer Scientific (Waltham, MA)	Cat. #: cd11b05 RRID: AB_2536483
Mouse anti-CD19-PE	Thermo Fischer Scientific (Waltham, MA)	Cat. #: MHCD1918 RRID: AB_10373840
Hamster anti-CD3-PerCP	Thermo Fischer Scientific (Waltham, MA)	Cat. #: 45-0031-82 RRID: AB_1107000
Rat anti-CD8-FITC	Thermo Fischer Scientific (Waltham, MA)	Cat. #: 11-0083-82 RRID: AB_657764
Rat anti-CD4-Pacific Blue	Thermo Fischer Scientific (Waltham, MA)	Cat. #: MCD0428 RRID: AB_1474222
Fungal, Bacterial and Virus Strains		
C. neoformans strain H99	Dr. Xiaorong Lin (Texas A&M University, College Station, TX)	N/A
C. neoformans strain H99-dsRed	Dr. Xiaorong Lin (Texas A&M University, College Station, TX)	N/A
C. burnetii RSA439 (Nine Mile Phase II)	Rocky Mountain Laboratories (Hamilton, MT USA)	(Samuel et al., 1985)
Chemicals, Peptides, and Recombinant Proteins		
Compound C	Sigma-Aldrich, Inc. (St. Louis, MO USA)	Cat. #: 171260-1MG
AICAR	Sigma-Aldrich, Inc. (St. Louis, MO USA)	Cat. #: A9978-5MG
Berberine	Cayman Chemical, Inc. (Ann Arbor, MI USA)	Cat. #: 10006427
RIPA buffer	G-Biosciences (San Diego, CA USA)	Cat. #: 786-489
Phosphatase inhibitor cocktail 2	Sigma-Aldrich, Inc. (St. Louis, MO USA)	Cat. #: P5726
Phosphatase inhibitor cocktail 3	Sigma-Aldrich, Inc. (St. Louis, MO USA)	Cat. #: P0044
Hypersep C-18 column	Thermo Fischer Scientific (Waltham, MA USA)	Cat. #: 60101-302
Critical Commercial Assays		
Phagocytosis Assay Kit (IgG FITC)	Cayman Chemical, Inc. (Ann Arbor, MI USA)	Cat. #: 500290
Fe-NTA column	Thermo Fischer Scientific (Waltham, MA USA)	Cat. #: 88300
Pierce ECL Plus chemiluminescence kit	Thermo Fischer Scientific (Waltham, MA USA)	*Cat. #: 32132X3*
Experimental Models: Cell Lines		
RAW264.7 cells	ATCC (Manassas, VA USA)	TIB-71
J774A.1 cells	ATCC (Manassas, VA USA)	TIB-67
B6J2 cells	Dr. J. Suttles (University of Louisville, Louisville, KY USA)	(Sag et al., 2008)

(*Continued on next page*)

Continued		
REAGENT or RESOURCE	SOURCE	IDENTIFIER
B6J2 cells (AMPKα-DN)	Dr. J. Suttles (University of Louisville, Louisville, KY USA)	(Sag et al., 2008)
MH-S cells	ATCC (Manassas, VA USA)	CRL-2019
Experimental Models: Organisms/Strains		
Mouse: C57B6 (Cg)-*Prkaa1*$^{tm1.1Sjm}$/J (Prkaa1$^{flox/flox}$)	Jackson Laboratories, Inc. (Bar Harbor, ME USA)	Stock No: 014141
Mouse: B6.129P2-*Lyz2*$^{tm1(cre)Ifo}$/J (Cre expression under Lyz2 promoter)	Jackson Laboratories, Inc. (Bar Harbor, ME USA)	Stock No: 004781
Oligonucleotides		
Primers for AIC amplification, see Table S6	This paper	N/A
Recombinant DNA		
Plasmids for recombinant DNA expression, see Table S5	This paper	N/A
Data Availability		
Proteome datasets generated in this study have been deposited in the PeptideAtlas database (http://www.peptideatlas.org/).	This paper	ID: PASS01011, Type: MSMS

CONTACT FOR REAGENT AND RESOURCE SHARING

Further information and requests for resources and reagents should be directed to and will be fulfilled by the Lead Contact, Paul de Figueiredo (pjdefigueiredo@tamu.edu).

EXPERIMENTAL MODEL AND SUBJECT DETAILS

Generation, Genotyping, and Characterization of Prkaa1$^{f/f}$-Lys2$^{cre/-}$ Mice

Animal research was conducted under the auspices of approval by the Texas A & M University Institutional Animal Care and Use Committee in an Association for Assessment and Accreditation of Laboratory Animal Care International-accredited animal facility. C57B6 (Cg)-*Prkaa1*$^{tm1.1Sjm}$/J (*Prkaa1*$^{flox/flox}$ mice) and B6.129P2-*Lyzs*$^{tm1(cre)Ifo}$/J (Cre expression under Lyz2 promoter) mice were purchased from Jackson Laboratory. To investigate the roles of *Prkaa1* in Cn infection, *Prkaa1*$^{f/f}$-*Lys2*$^{cre/-}$ (*Prkaa1*$^{-/-}$ CKO) mice were generated by breeding *Prkaa1*$^{flox/flox}$ mice (Jackson Laboratories, Inc.) with lysozyme M-Cre (LysM-Cre) transgenic mice (Jackson Laboratories, Inc.), in which the *Prkaa1* gene was specifically deleted in myeloid cells, including macrophages, monocytes, and neutrophils (Clausen et al., 1999). The CKO mice were genotyped using genomic DNA from tail vain to show the presence of floxed *Prkaa1* and *Cre* alleles (Figure S5). Western blot analysis using anti-AMPKα antibodies (Santa Cruz, Inc.) was performed on BMDMs from CKO and littermate control mice to show that that *Prkaa1* was efficiently disrupted in the CKO mice. Splenocytes from CKO mice were used to assess the levels of B cells (anti-CD19), T cells (anti-CD4 and anti-CD8) and CD11b^{+} cells compared to the control mice by staining with corresponding fluorochrome-labeled antibodies (BIOSS, Inc.) and performing flow cytometry analysis.

Bone-Marrow-Derived Macrophage and Alveolar Macrophage Harvest and Cultivation

Bone marrow cells were collected from the femurs of littermate control and *Prkaa1*$^{-/-}$ CKO mice, and cultivated in L929-cell conditioned media [DMEM medium containing 20% L929 cell supernatant, supplemented with 10% (v/v) FCS, penicillin (100 U/ml), and streptomycin (100 U/ml)]. After 3 days of culture, nonadherent precursors were washed away and the retained cells were propagated in fresh L929-cell conditioned media for another 4 days. For experimentation, cells were split in 24-well plates at a density of 2.5 × 10^5 cells per well in L929-cell conditioned media. Alveolar macrophages (AM) were isolated by bronchoalveolar lavage of control or *Prkaa1*$^{-/-}$ CKO male or female mice as previously described (Zhang et al., 2006). Each mouse was euthanized with a lethal dose of isoflurane inhalation and the chest cavity was dissected to expose the lungs and trachea. A 22-gauge catheter was inserted into the trachea and repeated lavages were performed, using 1 mL sterile ice-cold PBS, pH 7.4, each time, totaling 8 mL instilled per mouse. The lavage fluid was centrifuged at 300 g for 10 min. The pelleted cells were resuspended in RPMI 1640 complete medium (Zhang et al., 2006) and, in each well, 2.4 X 10^5 cells were plated on coverslips and cultured at 37°C with 5% CO_2.

METHOD DETAILS

Cryptococcus Strains, Immortalized Cell Culture, *Cryptococcus* Infection, and CFU Assay

Yeast forms of Cn cells were grown on YPD (Difco™) agar plates and maintained on the plates for no more than 1 week prior to experimentation. For infection, 1.0 mL of YPD broth was inoculated with a loop of Cn cells taken from a freshly streaked YPD plate. Cultures were then grown for ~12 hr with shaking at 37°C.

Several host cell lines were used for these studies. Murine MH-S, J774.A1 or RAW264.7 macrophages, or corresponding host cells depleted of AIC components (ULK1-KD, ATG13-KD or FIP200-KD) were employed. B6J2 cells or engineered lines that expressed *dominant negative variants of* AMPKα (Sag et al., 2008) were also used in some experiments. Mammalian cell lines were routinely incubated at 37°C in a 5% CO_2 atmosphere in DMEM supplemented with 10% FBS. Maintenance or preparation of host cells for Cn infection was performed as previously described (Qin et al., 2011). Tables S5 and S6 contan lists of plasmids, shRNAs and primers used in these studies.

In some infection experiments, antibody opsonized Cn was used. Briefly, approximately 1 X 10^7 Cn cells from a 12 hr liquid culture were washed three times in PBS, pH 7.4. The washed cells were then incubated with 10 μg/ml of anti-Cn monoclonal antibody [18B7]. The mixture was briefly mixed, and then incubated at 37°C with gentle shaking for 30 min. Next, the antibody treated cells were washed three times with ice cold PBS and resuspended in 1 mL of DMEM. These cells were used in infection experiments.

Infection of Host Cells with Ab-opsonized or Unopsonized Cn

Mammalian host cells were infected with Cn at a multiplicity of infection (MOI) of 10, unless otherwise indicated. For experiments where microscopy was used to analyze the phagocytosis or intracellular replication of Cn, host cells were first cultivated on 12 mm glass coverslips (Fisherbrand) contained in 24 well plates (Falcon). Next, the host cells were infected and then incubated at 37°C in a 5% CO_2 atmosphere. At the indicated time points post-infection, culture media was removed, and the infected cells were extensively washed (6 to 8 times) with PBS, pH 7.4, before being processed for analysis of phagocytosis or intracellular replication. In some experiments, fluconazole protection assays were used to measure the phagocytosis and intracellular replication of the pathogen as previously described (Qin et al., 2011). For assays that measured pathogen internalization by immunofluorescence microscopy, infected cells were fixed and processed as described (Qin et al., 2011) without adding Triton X-100 to the staining buffer.

Sample Preparation for Proteomic Analyses

RAW 264.7 macrophage cells were seeded in 6-well plates (10 plates per group) and cultured in DMEM supplemented with 10% FBS, Sodium pyruvate and nonessential amino acid (NEAA). The macrophage cells were infected with opsonized H99 at an MOI of 10. Mock-infected cells served as controls. Two hr post-infection, the infected cells were washed with cold PBS, pH 7.4, two times and then lysed with RIPA (Kim et al., 2012) buffer (G Biosciences) supplemented with protease inhibitor tablets (Sigma-Aldrich), phosphatase inhibitor cocktail 2 and phosphatase inhibitor cocktail 3 (Sigma-Aldrich). The lysed cells were collected, vortexed and twice clarified by centrifugation for 15 min at 4°C. The lysates were stored at −80°C. Portions of lysates were plated on YPD plates and no growth was observed confirming the absence of viable Cn in the lysate.

Sample Digestion

Five volumes of cold (−20°C) acetone were added to 1mg of sample and chilled at −20°C for 60 min. The sample was then centrifuged at 14,000 X g for 15 min and the supernatant decanted. 50 μL of 8M guanidinium HCl in 250 mM Tris-HCl, 10mM DTT, pH 8.6, was added to the pellet and incubated at 95°C for 10 min. The sample was then cooled to room temperature and 3.75 μL of 1M iodoacetic acid was added and allowed to react for 60 min in the dark. 0.5 μL of 2M DTT was then added to quench the reaction. The sample was diluted with 812 μL of 50mM Tris-HCl, pH 8.0, in 5mM $CaCl_2$. 125 μL of 25 mM acetic acid was then added directly to 20 μg of sequencing grade trypsin (Pierce), vortexed, and kept on ice. The protein mixture was added to the trypsin mixture, vortexed and incubated overnight at 37°C. Finally, trifluoracetic acid was added to a final concentration of 0.1% to quench trypsinolysis.

Phosphopeptide Enrichment

Samples were cleaned up using a hypersep C-18 column (60101-302, ThermoFisher) and then loaded on a Fe-NTA column (kit 88300, ThermoFisher), as described by the manufacturer. Eluted peptides were dried down in a speed vac to dryness. Phosphopeptides were resuspended in buffer A as per the manufacturer's instructions immediately prior to nanoflow liquid chromatography-tandem mass spectrometry (nanoLC-MS/MS).

NanoLC MS/MS Analyses

Peptide mixtures were analyzed by nanoLC-MS/MS using a nano-LC chromatography system (UltiMate 3000 RSLCnano, Dionex), coupled on-line to a Thermo Orbitrap Fusion mass spectrometer (Thermo Fisher Scientific, Inc., San Jose, CA) through a nanospray ion source (Thermo Scientific). A trap and elute method was used. The analytical column was an Acclaim PepMap 100 (75um X 15 cm) from Thermo Fisher Scientific. After equilibrating the column in 98% solvent A (0.1% formic acid in water) and 2% solvent B (0.1% formic acid in acetonitrile (ACN)), the samples (1 μL in solvent A) were injected onto the trap column and subsequently eluted

(400 nL/min) by gradient elution onto the C-18 column as follows: isocratic at 2% B, 0-5 min; 2% to 45% B, 2-37 min; 45% to 90% B, 37-40 min; isocratic at 90% B, 40-45 min; 90% to 2%, 45-47 min; and isocratic at 2% B, 47-60 min.

All LC-MS/MS data were acquired using XCalibur, version 2.1.0 (Thermo Fisher Scientific, Inc.) in positive ion mode using a top speed data-dependent acquisition (DDA) method with a 3 s cycle time. The survey scans (*m/z* 400-1,600) were acquired in the Orbitrap at 120,000 resolution (at *m/z* = 400) in profile mode, with a maximum injection time of 50 msec and an AGC target of 200,000 ions. The S-lens RF level was set to 60. Isolation was performed in the quadrupole with a 2.0 Da isolation window, and higher-energy collision dissociation (HCD) MS/MS acquisition was performed in profile mode using rapid scan rate with detection in the ion trap, with the following settings: parent threshold = 5,000; collision energy = 28%; maximum injection time = 250 msec; AGC target = 20,000 ions. Monoisotopic precursor selection (MIPS) and charge state filtering were on, with charge states 2-6 included. Dynamic exclusion was used to remove selected precursor ions, with a ± 10 ppm mass tolerance, for 60 s after acquisition of one MS/MS spectrum.

Database Searching and Analyses

Tandem mass spectra were extracted and charge states deconvoluted by Proteome Discoverer (Thermo Fisher Scientific, Inc., version 1.4.1.14). Deisotoping was not performed. All MS/MS spectra were searched against a Uniprot Murine database (version 08-11-2014) using Sequest. Searches were performed with a parent ion tolerance of 5 ppm and a fragment ion tolerance of 0.60 Da. Trypsin was specified as the enzyme, allowing for two missed cleavages. Fixed modification of carbamidomethyl (C) and variable modifications of oxidation (M) and phosphorylation were specified in Sequest. Quality metrics were as follows: (0) lowest confidence with no MS or MS/MS information matching library; (1) typically only had MS information based accurate mass and isotopic distribution matching, but did not have matched MS/MS spectra; (2) moderate confidence, typically had matched MS/MS spectra but poor MS (low level peptide or background interference) or high variance; (3) higher confidence with both MS and MS/MS information match, typically setting the coefficient of variance tolerance to 20% or lower, and appropriately shaped chromatographic peak shapes; (4) highest confidence and statistical relevance.

Bioinformatic Analyses

For comparative analysis of differentially phosphorylated proteins in response to infection by Cn and other bacterial or viral pathogens, we compared proteins with at least 1.5 fold changes at the times post-infection that were closest to those used in our Cn studies. Specifically, we analyzed the host response of *Shigella* at 2 hr.p.i. (Schmutz et al., 2013), *Francisella* at 2 hr.p.i. (Nakayasu et al., 2013), *Salmonella* at 8 hr.p.i. (Rogers et al., 2011), or HIV-1 at 1 m.p.i. (Wojcechowskyj et al., 2013). The corresponding protein IDs from these two studies were converted to UniProt IDs and their murine homologs were obtained from the InParanoid database (Sonnhammer and Östlund, 2015) for searching for the overlap between differentially phosphorylated proteins for our comparative analysis. Venn diagrams were plotted for proteins belonging to the enhanced or decreased phosphoproteomes. The p values for the significance of the overlap were calculated based on the hypergeometric test with the mouse genome as the background (24,231 protein-coding genes: http://www.informatics.jax.org/mgihome/homepages/stats/all_stats.shtml).

To identify Cn-responsive kinase substrate motifs, motif-x algorithm analysis was performed online (http://motif-x.med.harvard.edu/) to search for over-represented motifs within enhanced or decreased Cn-responsive phospho-peptides. The motif analysis was performed with 13 residues centered on phosphorylated serine or threonine and was filtered with the enrichment significance at 0.0001 and the number of occurrences adjusted from 3 to 10 based on the number of differentially phosphorylated peptides. Gene ontology (GO) figures were generated based on results obtained using Gene List Analysis tools (Mi et al., 2016) in the panther database (www.pantherdb.org). GO pie charts were manually generated using the output files for each analysis type. Results were also screened or sorted based on significance and fold changes where appropriate. Some ID conversions were done using python scripts written specifically for this work. Summary tables that include descriptions of the false discovery rates (FDR) and other statistical measures are included as Tables S4D–S4F.

Drug Treatments

In 48 well plates, murine macrophage J774.A1 or RAW264.7 cells were coincubated with assorted pharmacological compounds, including CC, AICAR or berberine for 3 hr. The media containing the compounds was then removed. For western blots, the compound-treated cells were washed 3 times with PBS, pH7.4, and lysed with RIPA buffer (G Biosciences), supplemented with a SigmaFAST protease inhibitor tablet (Sigma Chemical, Inc.) and phosphatase inhibitor cocktail 2 and cocktail 3 (Sigma Chemical, Inc.), and then harvested. The protein extracts were boiled for 5 min in sample buffer (Thermo Scientific, Inc.) containing 200 μM DTT, separated by SDS-PAGE, transferred onto PVDF membrane and blotted with the indicated antibodies. The blots were detected using an enhanced chemiluminescence kit (Pierce, Inc.). Blots were stripped and reprobed for assessment of protein levels using GAPDH (Glyceraldehyde 3-phosphage dehydrogenase) as a loading control. Densitometry of the blots was performed using ImageJ (http://rsbweb.nih.gov/ij/). For CFU assays, the treated cells were washed with fresh drug-free medium 3 times, and then infected with *C. neoformans* as described above. To test the effects of the examined chemicals on the activity or expression of fungal virulence determinants, we measured urease activity and capsule as described (Feder et al., 2015; Kwon-Chung et al., 1987).

Retrovirus Infection and shRNA-Catalyzed Depletion of Host Proteins

The pSuperRetro retrovirial vector system (OligoEngine, Inc.) was used in accordance with the manufacturer's instructions to knockdown target gene expression in murine cells. The oligonucleotides used for shRNA construction to knockdown the expression of

mouse genes and the accompanying references are listed in Table S6. Transfection was performed in 6-well plates containing 1-3 X 10^5 RAW264.7 or B6J2 cells. Clones in which the insert was stably integrated were selected with puromycin. To verify that the targeted proteins were in fact depleted, western blot (Towbin et al., 1979) using antibodies directed against these proteins was performed. All Westerns were performed in triplicate and representative findings are shown.

Microscopy

Prevoiusly described immunofluorescence microscopy staining and imaging methods were used to determine the subcellular localization of host AIC components in infected host cells (Qin et al., 2011). For nonpermeable immunofluorescence microscopy, infected cells were fixed and processed as described (Qin et al., 2008) without adding Triton X-100 in the staining buffer. For regular fluorescence or immunofluorescence microscopy, infected cells were processed as previously described (Qin et al., 2008; 2011). Samples were observed on a laser scanning confocal microscope or on a confocal fluorescence microscope (ECLIPSE Ti, Nikon). Confocal images (1,024 × 1,024 pixels) were acquired and processed with NIS elements AR 3.0 software (Nikon) and assembled with Adobe Photoshop CS3 (Adobe Systems, San Jose, CA). Digital image analysis and quantification was performed as previously described (Qin et al., 2011). Findings from our subcellular localization analyses were not an artifact of secondary antibody cross reactivity with host or pathogen components because negligible fluorescence signal was observed when infected cells were stained with secondary antibodies alone, or the pathogen alone was stained with the antibodies used in the experiments. Preparation of samples for electron microscopy was performed using a previously described approach with minor modifications (Bozzola, 2007). Briefly, RAW 264.7 cells were infected with Cn. At 2 hr.p.i., cells were washed 3-5 times in 1X PBS, pH 7.4, and fixed in 1.5% glutaraldehyde in 0.1 M Na cacodylate, pH 7.4 for 1-2 hr at room temperature (RT). Fixative was replaced with 0.5% glutaraldehyde in 0.1 M Na cacodylate, pH 7.4 and cells were stored overnight at RT. Cells were harvested using a cell scraper, pelleted and washed gently with 100 mM 100 Na cacodylate, pH 7.2. After the last wash, cells were post-fixed with ice cold 1% OsO4 in 100 mM NaCacodylate, pH 7.2 on ice for 1 hr. Pellets were washed again carefully 3 times with 100 mM NaCacodylate, pH 7.2, on ice. The cells were dehydrated in a graded series of EtOH and rinsed several times each with 75%, 95%, 100% ethanol. Finally, the samples were rinsed 3 times with 100% EtOH and dehydrated with 100% propylene oxide (3 gentle washes). The pellet was incubated with 1:1 mixture of 100% propylene oxide:Spurr's resin for 30-60 min. Finally, the cells were embedded in Spurr's resin and thin sections were cut with a Leica EM UC6 ultramicrotome. Sections were stained with Reynold's lead citrate and aqueous uranyl acetate and visualized with an FEI Morgagni 268 transmission EM. Images were captured with an AMT XR50 camera. All images are representative of fields from triplicate experiments in which at least 300 infected host cells were examined.

Immunoblotting Analysis

Preparation of protein samples and western blot analysis were performed as described previously (Qin et al., 2011). Densitometry of blots was performed using the ImageJ (http://rsbweb.nih.gov/ij/) software package. All Westerns were performed in triplicate and representative findings are shown.

Ex Vivo or In Vivo Stimulation and Phosphorylation Analyses

Phosphoflow cytometry was performed using a protocol modified from Peter O. Krutzik et al. (Krutzik and Nolan, 2003). For ex vivo stimulation experiments, spleens were removed, minced, digested in collagenase type IV (Worthington) for 30 min and then washed in PBS, pH 7.4 twice followed by lysis of red blood cells. Cells were then passed through a 70-μm pore size mesh, pelleted, and resuspended at room temperature in RPMI 1640 containing 10% FBS, penicillin (100 U/ml), streptomycin (100 μg/ml), L-glutamine and essential amino acids. Cells were cultured at 37°C for 3-4 hr and then infected or treated with 10 MOI of Cn or Berberine (20 μM, Sigma-Aldrich, Inc.) or PBS, pH 7.4, for 30 min before formaldehyde fixation by directly adding the fixative (1.6% final concentration) to the treated cells for 10 min. For in vivo stimulation experiments, C57BL/6 mice were mock- infected or infected with 1 X 10^7 Cn cells via intraperitoneal delivery. Six hr later, spleens were harvested, dissociated and immediately fixed by homogenization in 1.6% paraformaldehyde for 10 min.

The host cells obtained from either *ex-vivo* or in vivo stimulation were pelleted and permeabilized by resuspension in ice-cold methanol, and incubated for 30 min at 4°C. The cells were then washed twice with FACS buffer (PBS, pH 7.4, with 1% BSA and 0.05% Sodium Azide). Next, 10^6 cells were stained with a mixture of fluorescently labeled antibodies against CD11b (eBioscience, Inc.) and phospho-AMPK (pAMPKα-Thr172) (Bioss, Inc.) or phosphor-ULK1 (pULK1-Ser555) (Bioss, Inc). Cells were stained for 30-45 min at 4°C and then washed before data acquisition on either a BD FACS Aria III or Fortessa X-20. FACS analysis was performed using Flowjo software (Tree Star Inc., OR USA).

To assess fungal replication in different knock down (KD) cell lines by flow cytometry, we used the method described by Nicola et. al. (Nicola et al., 2011) with some minor modifications. Control and AIC depleted or inactivated cells in 6 well plates were stained with 1 μM 9-*H*-(1,3-dichloro-9,9-dimethylacridin-2-one-7-yl)-succinimidyl ester (DDAO-SE) in PBS, pH 7.4, for 10 min. Cells were washed twice with PBS, pH 7.4, and then placed in DMEM containing 10% heat-inactivated fetal bovine serum (FBS), nonessential amino acids and sodium pyruvate. Cn cells grown overnight in YPD medium were washed twice with PBS, pH 7.4, and stained with 1 μm 5-chloromethylfluorescein diacetate (CMFDA) for 30 min at 37°C. Subsequently, the stained cells were washed twice with PBS, pH 7.4, and antibody-opsonized (10 μg/ml anti-capsular IgG1 monoclonal antibody 18B7) for 30 min. DDAO-SE stained control and KD cells were then infected with CMFDA labeled and antibody-opsonized Cn. At various times post-infection, Uvitex-2B dye (0.01% in PBS, pH 7.4) was added to the wells for 1 min to stain extracellular Cn. Wells were washed 4-6 times to remove residual dye and Cn.

Finally, the infected cells were fixed by adding 1.6% paraformaldehyde to the wells and incubated for 20 min. The fixed cells were scrapped using rubber policemen (Fisherbrand, Inc.) and the fixative was removed by washing once with PBS, pH 7.4. Duplicate wells that received similar treatments were stained with trypan blue to assess cell viability.

Phagocytosis Assays

Phagocytosis assays were performed using a Phagocytosis Assay Kit (IgG FITC) as per the manufacturers instructions (Cayman Chemical, Inc.). Briefly, latex beads (coated with FITC-labeled rabbit-IgG) were incubated (in 96 well plates) with RAW264.7 cells ($\sim$5x10^4 cells/well) expressing scrambled shRNA sequences (control) or shRNAs that depleted target AIC proteins. At various times post-infection, the cells were washed 2 times with prewarmed PBS and then washed briefly with Trypan blue, to quench the fluorescence of cell surface-associated beads. Finally, the cells were imaged and analyzed by confocal microscopy, to determine the average number of internalized beads per host cell. All data were derived from six biologically independent experimental replicates.

Animal Infections with Cn and Tissue Analysis

Mice from CKO and littermate control groups were infected intraperitoneally (i.p.) or via pulmonary instillation (p.i.) with 10^5 CFU of Cn. Fourteen days later mice were euthanized and the Cn burden was assessed in spleen, lung, liver and brain for i.p. infected mice and lung and brain for p.i. infected mice. A portion of the tissue was fixed and paraffin embedded for histopathological examination following H&E staining. To evaluate the effects of selective pharmacological inhibition of AMPK on Cn infection of mice, groups (n = 5) of 6-week-old female C57BL/6 mice (Jackson Laboratory, Inc., Bar Harbor, Maine) were treated i.p. with compound C (Sigma-Aldrich, 20 mg/kg) or vehicle and 24 hr later infected intraperitoneally with 10^7 CFU of Cn. Lung, liver and spleen were harvested 6 hr post-infection (h.p.i.) to assess the tissue burden of Cn by serially diluting and plating the tissue homogenates in YPD-agar (Yeast, Peptone, Dextrose) plates followed by incubation at 37°C in 5% CO_2 for 48 hr. Cytokines from culture supernatants were analyzed using commercially available ELISA kits (R&D Systems, Inc., Minneapolis, MN USA or BioLegend, Inc., San Diego, CA) as previously described (Gomez et al., 2013).

Infection of Host Cells with *Coxiella burnetii*

Coxiella burnetii strain RSA439 (Nine Mile Phase II) was maintained axenically in ACCM-2 broth as previously described (van Schaik et al., 2017). Primary bone marrow derived macrophages (BMDM) were prepared from control or *Prkaa1*$^{-/-}$ CKO mice as previously described (Chong et al., 2008). To infect BMDMs with *C. burnetii*, the bacteria were enumerated by TaqMan qPCR using primers and probe directed against the *IS1111* sequence (van Schaik et al., 2017) and applied to the cells on ice at an MOI of 50. The inoculated BMDMs were centrifuged at 500x*g* for 10 min at 4°C, and then shifted to a water bath at 37°C, 5% CO_2 to synchronize bacterial uptake. After 1 hr of incubation, the cells were washed 3 times with DMEM to remove excess inoculum; the media was replaced with complete macrophage medium (DMEM supplemented with 10% FBS, and 10% L929 conditioned medium), and returned to the incubator for a total of 7 days. The culture medium was replaced daily, and infected cells were collected at 1, 4, and 7 days post-infection for genomic DNA isolation and enumeration of bacteria by TaqMan qPCR. Three independent infections were performed, and all samples were collected in triplicate.

QUANTIFICATION AND STATISTICAL ANALYSIS

The figure legends describe the exact number of independent replicates, or animals per group, that were analyzed in each quantitative experiment. The presented quantitative data represent the mean ± standard deviation (SD) from at least three biologically independent experiments. To easily compare results from independent experiments, the data from controls were normalized as 1 or 100%. The significance of the data was assessed using the Student's t test. For the proteomic experiments, Log2 fold changes were calculated and results were screened to meet the threshold for selection. Screening was done to verify that only expression that had complete data were included in the final lists. Various in-house python code scripts were written to automate this screening process.

DATA AND SOFTWARE AVAILABILITY

Proteomic datasets generated in this study have been deposited in the PeptideAtlas database (http://www.peptideatlas.org/). The accession number for the combined dataset reported in this paper is Peptide Atlas: PASS01011.